Table 1. Clinical data for patients enrolled in Illumina sequencing analysis.

Patient	Sex	Age	Biopsy finding[a]	T-bil (mg/dl)	ALT (IU/l)	ALP (IU/l)	Albumin (g/dl)	PT-INR	ANA	AMA	M2 (index)	HBV-DNA (Log copies/ml)	HCV-RNA (LogIU/ml)	Past treatment[b]
PBC-1	M	60	II	0.5	36	404	3.8	1.00	-	1:80	128			URSO (−)
PBC-2	M	65	I	1.2	54	485	4.1	1.05	-	1:160	125			URSO (−)
PBC-3	F	61	II	1.2	38	478	4.0	0.97	-	1:20	89.5			URSO (−)
PBC-4	F	51	III	0.8	71	798	3.8	0.96	-	-	47.9			URSO (−)
PBC-5	F	62	II	0.6	26	407	4.0	0.99	-	1:20	102			URSO (−)
PBC-6	F	61	I	0.6	38	527	4.2	0.91	-	-	111.4			URSO (−)
PBC-7	F	55	II	1.0	53	800	4.2	1.02	1:80	-	89.9			URSO (−)
PBC-8	F	52	II	0.9	28	525	3.7	0.94	1:80	-	-			URSO (−)
PBC-9	F	72	I	1.1	42	666	3.4	1.00	-	1:80	143.9			URSO (−)
PBC-10	F	64	I	0.7	38	513	4.0	0.88	>2561	1:80	79.4			URSO (−)
CH-C-1	M	57	2	0.6	22	240	4.4	0.91					5.4	IFN (+)
CH-C-2	F	55	3	1.5	73	403	4.0	1.06					5.1	IFN (+)
CH-C-3	F	61	1	1.1	12	179	4.2	1.11					5.2	IFN (+)
CH-C-4	F	49	2	0.8	42	261	3.6	1.05					6.3	IFN (−)
CH-C-5	F	53	2	0.8	27	257	4.0	0.93					6.9	IFN (+)
CH-B-1	F	35	1	0.7	585	283	4.1	1.03				9.1		NA (−)
CH-B-2	F	72	2	0.9	64	211	3.8	1.03				3.4		NA (−)
CH-B-3	F	38	2	0.8	283	268	3.1	0.99				8.8		NA (−)
CH-B-4	F	43	3	0.6	87	239	3.7	1.01				7.4		NA (−)
CH-B-5	M	47	1	0.6	40	156	4.1	1.12				5.9		NA (−)
Healthy-3	M	37		0.6	24	252	4.2	1.02						
Healthy-4	F	49		0.7	21	274	4.1	1.08						
Healthy-5	F	33		0.6	18	173	3.9	1.12						
Healthy-7	M	26		0.8	35	218	4.3	1.08						
Healthy-8	M	28		0.9	22	238	4.2	1.04						

[a]We used the Scheuer score in PBC and fibrosis score of histological activity index (HAI) in CH-B and CH-C [53] [54] [55].
[b]URSO is the abbreviation for ursodeoxycholic acid, IFN for interferon and NA for nucleos(t)ide analogue.
doi:10.1371/journal.pone.0066086.t001

Table 2. The number of small RNAs in serum detected by Illumina sequencing.

		Cutadapt		Mapping (miRBase)		Mapping (hg19)	
Sample	Total	No. of read	% read	No. of read	% read	No. of read	% read
PBC-1	9,996,912	5,912,672	59.14	582,682	9.85	5,195,131	87.86
PBC-2	17,103,184	8,147,153	47.64	837,575	10.28	6,484,515	79.59
PBC-3	11,731,105	9,001,730	76.73	873,985	9.71	5,414,933	60.15
PBC-4	12,785,162	10,700,147	83.69	1,463,341	13.68	8,227,422	76.89
PBC-5	14,732,479	9,138,080	62.03	1,125,157	12.31	7,317,178	80.07
PBC-6	12,139,379	7,256,738	59.78	1,274,462	17.56	5,612,279	77.34
PBC-7	12,895,734	10,107,477	78.38	1,067,578	10.56	7,826,537	77.43
PBC-8	18,786,941	11,711,844	62.34	967,802	8.26	8,323,607	71.07
PBC-9	11,852,431	8,980,873	75.77	1,141,912	12.71	7,593,581	84.55
PBC-10	18,224,562	12,752,337	69.97	756,930	5.94	8,912,212	69.89
CH-C-1	10,874,814	7,820,291	71.91	2,870,316	36.70	6,924,685	88.55
CH-C-2	10,242,500	8,138,815	79.46	3,250,159	39.93	6,976,754	85.72
CH-C-3	19,183,649	12,135,107	63.26	1,878,487	15.48	9,056,579	74.63
CH-C-4	18,750,568	15,952,136	85.08	1,877,654	11.77	14,829,719	92.96
CH-C-5	12,702,304	10,306,186	81.14	1,592,422	15.45	9,269,394	89.94
CH-B-1	5,861,013	4,732,185	80.74	1,126,751	23.81	3,708,378	78.37
CH-B-2	7,164,871	5,937,732	82.87	1,213,392	20.44	5,076,436	85.49
CH-B-3	7,029,349	6,357,274	90.44	858,562	13.51	5,378,310	84.60
CH-B-4	8,077,025	6,788,987	84.05	1,581,475	23.29	6,142,836	90.48
CH-B-5	10,255,895	9,101,104	88.74	1,952,400	21.45	7,687,217	84.46
Healthy-3	11,111,254	7,843,011	70.59	1,248,499	15.92	6,778,655	86.43
Healthy-4	12,449,813	10,690,833	85.87	2,410,128	22.54	9,204,163	86.09
Healthy-5	13,597,339	8,914,365	65.56	2,214,635	24.84	6,571,819	73.72
Healthy-7	11,351,494	9,825,442	86.56	1,880,266	19.14	8,618,696	87.72
Healthy-8	14,349,933	12,891,294	89.84	2,320,100	18.00	11,618,231	90.12
Total	313,249,710	231,143,813	73.79	38,366,670	16.60	188,749,267	81.66

doi:10.1371/journal.pone.0066086.t002

BIOCARTA showed that the genes of catenin (cadherin-associated protein), alpha 1 and similar to breast cancer anti-estrogen resistance 1 predicted target genes of the listed miRNAs, and played a role in cell-to-cell adhesion signaling pathway (Figure S1). The KEGG pathway indicated that the genes of baculoviral IAP repeat-containing 2, protein phosphatase 3 catalytic subunit beta isoform and tumor necrosis factor ligand superfamily member 10 were related to apoptosis (Figure S2).

Discussion

MiRNA changes in the liver have been reported in diseases such as HCC or chronic viral hepatitis. However, there is only limited information about their detection in blood and their correlations in PBC patients. The current study provides the first evidence that PBC is associated with altered miRNA expression. We have demonstrated that a number of miRNAs, especially hsa-miR-505-3p and miR-197-3p, were significantly differentially expressed in patients with PBC, leading to a unique miRNA expression profile in the diseased liver. Recently, many studies have examined several PBC associations with genes and there have been significant differences in the genetic risk loci reported [21] [30]. Therefore more carefully constructed studies will be needed to clarify, the pathogenesis of PBC, and the study of these differentially expressed miRNAs could serve in identifying biomarkers or lead to a better understanding of the underlying molecular mechanism that perpetuates PBC.

In our study, miRNA Illumina deep sequencing was first used to screen 10 PBC patients' sera. We were able to match the sample's sex because of particular importance for X-linked miRNA [31]. Then, qRT-PCR was used to confirm the result of deep sequencing.

Quantitative differential expression analysis identified a 81-miRNA signature distinguishing PBC, CH-C, CH-B and healthy controls. A hierarchical clustering analysis was performed utilizing the 81-miRNAs and their patterns separated the PBC from viral hepatitis and healthy controls. In addition, there were three subgroups (PBC-1,2,4,5, PBC-3,6,10 and PBC-7,8,9) in the PBC cluster. When comparing the subgroups, the PBC-3, 6,10 group showed an expression pattern that differed from those of the other two subgroups. As for the clinical background, PBC-6 patient that had been infected with hepatitis B virus were HBsAg negative and anti-HBc and anti-HBs positive, and PBC-10 patient had positive antinuclear antibodies (ANA) titers of 1:2560 or greater, while other patients had no serological evidence of HBV infection and no positive ANA titers of 1:160 or greater. However, there was no clear difference between the three subgroups in terms of the clinical stage. At present, there is no conclusive proof whether

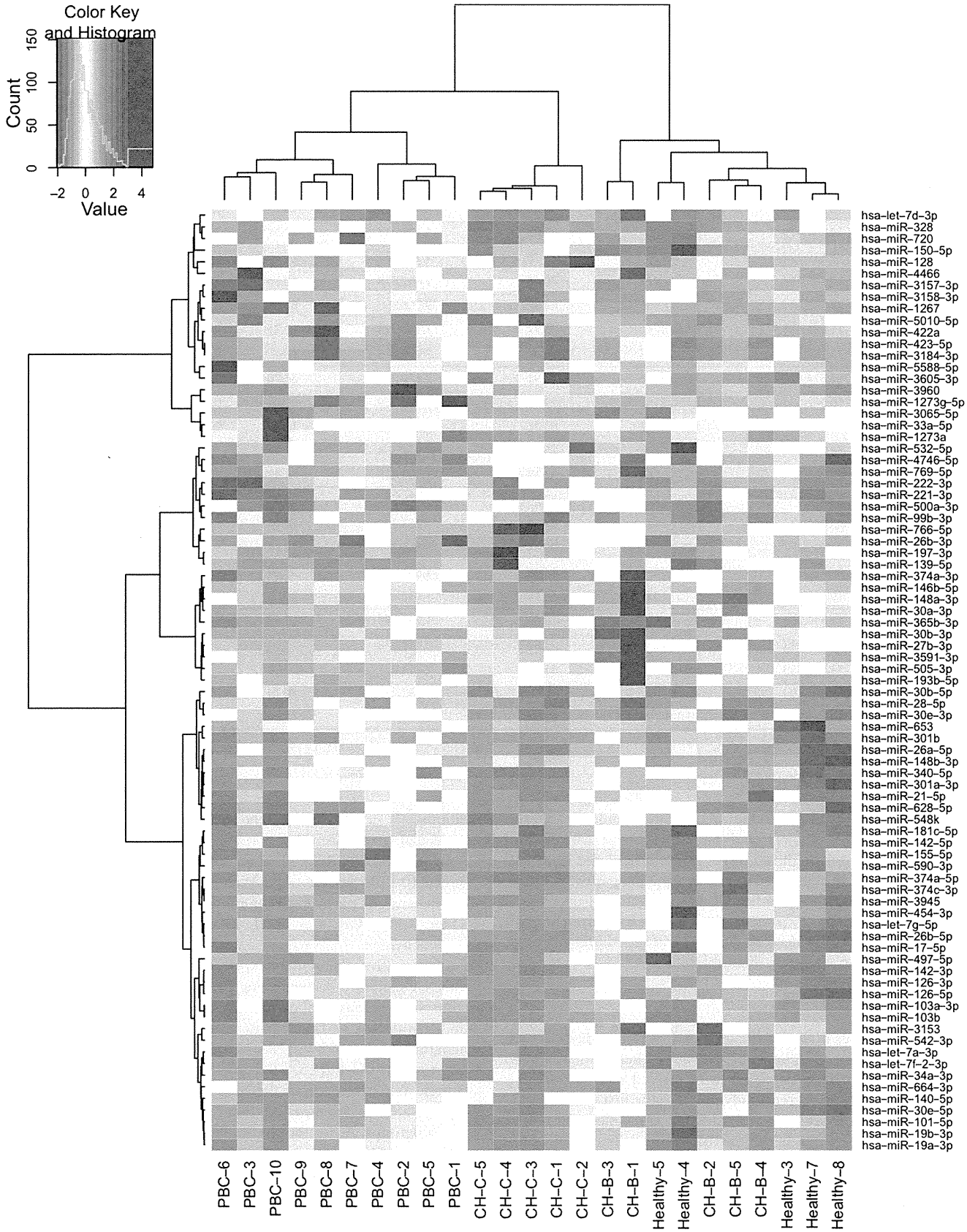

Figure 1. Heat map and hierarchical clustering. Individual miRNA expression were calculated by R platform and heat map was computed and described using a function of heatmap.2 in gplots. It uses hierarchical clustering with Euclidean distance; Pearson Linear Correlation and Ward's method to generate the hierarchical tree [56]. ANOVA was applied to extract differentially expressed miRNAs and adjustment of the p-value by

multiple comparisons was performed by calculating FDR. Those miRNAs with FDR<0.1 were presented. The red indicates high level of miRNA expression and the blue shows low.
doi:10.1371/journal.pone.0066086.g001

clinical or pathological differences can be found in clustering subgroups.

Nine miRNAs were confirmed to be significantly differentially expressed between the PBC group and viral hepatitis group or healthy control by Illumina deep sequencing. Among these 9 miRNAs, the serum levels of hsa-miR-505-3p and miR-197-3p were significantly lower in patients with PBC than in those with viral hepatitis and healthy controls, hsa-miR-139-5p was lower in patients with PBC than in those with viral hepatitis and miR-500a-3p were lower in patients with PBC than in healthy controls. Of note, we conducted qRT-PCR on the sera of some PBC who had already been treated with ursodeoxycholic acid. The serum levels of miRNA showed improvements in some samples (data not shown). Accordingly, quantifying these miRNAs may yield reliable diagnostic information. However, one problem is that the quantification of miRNA in this study used standardization by the total numbers of 1,000,000 reads in the deep sequencing or a comparative method in qRT-PCR. In other words, it was assumed that the same amount of miRNA was contained in each serum sample. Therefore, if one miRNA is quantified in a single specimen, we will not be able to accurately assess the result.

Specific circulating miRNA profiles have been reported for various diseases [32] [5] [33] [34] [35]. These circulating miRNA profiles have been described as correlating with differentially expressed miRNA in diseased tissue, such as liver injured by drugs or stomach afflicted with gastric cancer [36] [37]. Moreover, some disease-specific profiles can inform both the diagnosis and prognosis [38] [39]. Therefore, to determine if any of these diferentially expressed miRNAs could lead to better understanding of the molecular mechanism that perpetuates PBC, we examined for gene targets that may be reflected by this particular miRNA expression signature. Of the several target prediction algorithms prepared, we selected mirror 2.0. There has been evidence that a seed region of miRNA positioned within a limited range in the 3′ UTR of a target gene degrades the mRNA function [40]. We predicted 75 genes as targets for 9 differentially expressed miRNAs and conducted a functional analysis of DAVID. This analysis revealed that the genes of catenin (cadherin-associated protein), alpha 1 and similar to breast cancer anti-estrogen resistance 1 predicted target genes of the listed miRNA and played a role in cell-to-cell adhesion signaling, and the genes of baculoviral IAP repeat-containing 2, protein phosphatase 3 catalytic subunit beta isoform and tumor necrosis factor ligand superfamily member 10 were related to apoptosis. The onset of autoimmune disorders with PBC can be linked to apoptosis. A previous report described that the expression of TRAIL receptors is up-regulated by an increased bile acid level and that the serum level of soluble TRAIL is elevated, which may be involved in the development and progression of PBC [41,42]. However, further work will be required so that these miRNAs can serve not only as biomarkers but also for the elucidation of the pathogenesis of PBC.

GO analysis provides representations of biological annotations using precisely defined terms [43]. A previous report has described a number of genes involved in the signaling, regulation of I-kappaB kinase/NF-kappaB cascade and homeostasis that are associated with PBC [44] [45,46]. Additionally, our study indicated the biological processes, cellular component and molecular functions affected by the target genes included those associated with cell or membrane fraction, various kinds of ion binding and protein serine/threonine phosphatase complex, all of which are potentially related to PBC. Further studies will need to examine the relationship between differentially expressed miRNAs, both in serum and liver tissue, and target genes, which may provide more insights into the role of miRNAs in the pathology of PBC.

In conclusion, our results indicate that sera from patients with PBC have a unique miRNA expression profile compared to viral hepatitis and healthy controls and down-regulated expression of hsa-miR-505-3p and 197-3p may represent new clinical biomarkers in PBC. This study suggests that the amounts of miRNAs in serum have potential as diagnostic and prognostic biomarkers for PBC.

Materials and Methods

Patients and sample processing

We included sera of 10 patients with PBC who were treatment-naïve, sera of 5 patients with CH-B, sera of 5 patients with CH-C and sera of 5 healthy controls in this study. Initially these serum samples were enrolled to be analyzed by the Illumina miRNA deep sequencing (Illumina). The diagnosis of all cases was based on internationally established criteria [23].

Library preparation and Illumina sequencing

A ten ml venous sample was collected from each participant. The whole blood was separated into serum and cellular fractions by centrifugation at 2,500 r.p.m. for 10 min, followed by 10 min centrifugation at 10,000 r.p.m. to completely remove cell debris. The supernatant serum was stored at −20°C until analysis. Total RNA was extracted from 800 µl of serum using Trizol LS (Invitrogen, Carlsbad, CA). The libraries were constructed from total RNA using the TruSeq Small RNA Sample Prep Kit (Illumina, San Diego, CA) following the manufacturer's protocol. Briefly, RNA 3′ and 5′ adapters were ligated to target microRNAs in two separate steps. Reverse transcription reaction was conducted to the ligation products to create single stranded cDNA. The cDNA was amplified by PCR using a common primer and a primer containing the index sequence. One µl of each library was loaded on an Agilent Bioanalyzer (Agilent, Santa Clara, CA) to check the size, purity, and concentration. Libraries were sequenced on an Illumina GA IIx (SCS 2.8 software; Illumina, SanDiego, CA), with a 32-mer single end sequence. Image analysis and base calling were performed using RTA 1.8 software.

Sequence and statistical analysis

Raw miRNA sequence reads were conducted as a quality check and the 3′ and 5′ adapter sequences were removed by cutadapt while discarding reads shorter than 20 nucleotides [27]. The sequence reads were mapped with miRBase (Release 18) and UCSC (hg19) by use of bwa (0.5.9-r16), allowing one nucleotide base mismatch [47] [48].

Digital expression levels were normalized by taking into account the length of miRNAs and the total number of miRNA reads generated in each library using TMM normalization [28]. Read counts of each identified miRNA was normalized to the total number of miRNA reads, and then the ratio was multiplied by a constant set to 1×10^6 in this study. ANOVA was applied to extract differentially expressed miRNAs among the four groups. Adjustment of the p-value by multiple comparisons was performed by

Table 3. Differentially expressed miRNAs in serum from PBC patients compared with the second group (CH-C, CH-B, Healthy).

miRNA	Expression	PBC	CH-C	CH-B	Healthy	Fold change	p-value
		The mean no. of reads ±SE	The mean no. of reads ±SE	The mean no. of reads ±SE	The mean no. of reads ±SE		
hsa-miR-1273g-5p	Up	6.79±0.50	1.88±0.26	0.51±0.10	1.21±0.08	3.61	9.93E-03
hsa-miR-33a-5p	Up	6.19±1.59	0.10±0.04	1.58±0.23	2.20±0.18	2.82	4.07E-03
hsa-miR-3960	Up	11.26±0.59	4.85±0.51	3.63±0.27	1.86±0.24	2.32	4.27E-03
hsa-miR-766-5p	Down	0.17±0.04	2.92±0.53	1.55±0.10	0.64±0.12	0.27	4.61E-03
hsa-miR-505-3p	Down	5.05±0.22	16.23±0.89	26.81±3.99	16.73±1.54	0.31	3.40E-03
hsa-miR-30b-3p	Down	0.41±0.08	3.76±0.38	8.77±1.00	1.30±0.26	0.31	1.01E-03
hsa-miR-139-5p	Down	19.73±0.77	77.72±9.44	61.29±6.57	82.86±6.06	0.32	6.86E-03
hsa-miR-197-3p	Down	226.99±10.32	1067.05±106.41	589.88±60.38	823.16±66.17	0.38	7.76E-03
hsa-miR-500a-3p	Down	36.01±1.66	74.61±1.95	86.52±5.35	99.59±3.00	0.48	2.29E-03

doi:10.1371/journal.pone.0066086.t003

calculating FDR [49]. Those miRNAs with FDR<0.1 were extracted as differentially expressed and used in the following analysis. Hierarchical clustering was performed using an R platform and a heat map described as using a function of heatmap.2 in gplots [50].

qRT-PCR validation study

In addition to 25 samples analyzed by Illumina sequencing, five more serum samples of CH-B, CH-C and healthy controls (a total of 10 samples in each group) were used in qRT-PCR validation study. We followed the protocol previously reported by Mitchell *et al.* to determine the endogenous miRNA levels with spiked-in miRNA. Spiked-in miRNA was designed against *Caenorhabditis elegans* microRNA-39 (cel-miR-39) (5′- UCA CCG GGU GUA AAU CAG CUU -3′) and was synthesized by Sigma Aldrich Japan [32]. After total RNA isolation from 300 µl serum, reverse transcription was conducted using a TaqMan miRNA RT kit for identification of the cel-miR-39 expression (Applied Biosystems) with 5 fmol/µl for the internal control. qRT-PCR were conducted for detection of hsa-miR-1273g-5p, miR-505-3p and miR-139-5p in 20 µl PCR reactions using TaqMan MicroRNA assay with StepOne Plus detection system at 50°C for 2 min and 95°C for 10 min, followed by 40 cycles of 95°C for 15 s and 60°C for 1 min (Applied Biosystems). For detection of hsa-miR-33a-5p, miR-3960, miR-766-5p, miR-30b-3p, miR-197-3p and miR-500a-3p expression, we used the Exiqon system. Total RNA was reverse transcribed using the miRCURY LNA™ Universal RT miRNA PCR, Polyadenylation and cDNA synthesis kit (Exiqon). cDNA diluted 50× was assayed in 10 µl PCR reactions according to the protocol for miRCURY LNA™ Universal RT miRNA PCR with StepOne Plus detection system at 95°C for 10 min, followed by 40 cycles of 95°C for 10 s and 60°C for 1 min (Exiqon). The data were analyzed by the $2^{-\Delta\Delta Ct}$ method.

Statistical methods

Expression levels of the selected miRNAs detected by qRT-PCR were normalized to cel-miR-39 and presented as the fold-change ($2^{-\Delta\Delta Ct}$) above the control (CH-C-5): $\Delta\Delta Ct = (Ct_{miRNA}\text{-}Ct_{cel\text{-}miR\text{-}39})_{patients}\text{-}(Ct_{miRNA}\text{-}Ct_{cel\text{-}miR\text{-}39})_{CH\text{-}C\text{-}5}$. Results for normally distributed continuous variables are given as means (±standard errors of the mean) and compared between groups by Student's t-test. Results for non-normally distributed continuous variables are summarized as medians (interquartile ranges) and were compared by Mann-Whitney U test.

In silico analysis of miRNA target gene

For computational prediction of miRNA target genes, we used an algorithm: miRror 2.0 (June 2010 release, http://www.proto.cs.huji.ac.il/mirror/) [51]. MiRror 2.0 encompasses most of the available miRNA-target prediction tools covering human miRNAs. The algorithms used are collectively called miRNA-target prediction databases (MDBs): (i) PITA (Kartez); (ii) PicTar 4 (Krek); (iii) TargetRank (Nielsen); (iv) TargetScan (Lewis); (v) microCosm (John); (vi) miRanda (Betel); (vii) DIANA-microT (Maragkakis); (viii) MirZ (Hausser); (ix) miRDB (Wang); (x) RNA 22 (Miranda); (xi) MAMI (Sethupathy); (xii) miRNAMap2 (Hsu). The number of candidate genes and the number of miRNAs are indicated for each of the major MDBs. We selected as the search mode: miR2Gene; and as the search parameters of organism: human; and of selected tissue: all. Advanced parameters were inputted, cutoff: 0.01; database hits: 2; and target counts: 3. We created a list of common target genes for miRNAs. Then, these common targets were annotated by an annotation tool at the DAVID v6.7 (January 2010 release, http://david.abcc.ncifcrf.

Table 4. Clinical information of patients enrolled in the validation study.

	PBC (n = 10)	CH-C (n = 10)	CH-B (n = 10)	Healthy (n = 10)
Male/Female	2/8	4/6	6/4	6/4
Age range	51–72	47–70	27–72	26–62
Histological findings[a]				
Scheuer score	I (4) II (5) III (1)			
HAI		1 (1) 2 (8) 3 (1)	1 (3) 2 (4) 3 (3)	
T-bil (mg/dl)[b]	0.9 (0.5–1.2)	0.9 (0.6–1.5)	0.8 (0.5–1.1)	0.8 (0.6–1.0)
ALT (IU/l)[b]	42.4 (26–71)	47.1 (12–193)	139.1 (13–585)	25.8 (18–38)
ALP (IU/l)[b]	560.3 (404–800)	238.7 (167–403)	221.7 (111–319)	230.4 (148–302)
Albumin (g/dl)[b]	3.9 (3.4–4.2)	4.0 (3.5–4.2)	3.9 (3.7–4.4)	4 (3.8–4.3)
PT-INR[b]	0.97 (0.88–1.05)	1.02 (0.91–1.11)	1.07 (0.99–1.18)	1.07 (1.02–1.13)
AMA positivity	6			
M2 positivity	9			
HBV-DNA (Log copies/ml)[b]			6.2 (3.4–9.1)	
HCV-RNA (LogIU/ml)[b]		6.4 (5.1–7.3)		

[a]The numbers of patients are indicated in the parentheses.
[b]The range of laboratory data is indicated in the parentheses.
doi:10.1371/journal.pone.0066086.t004

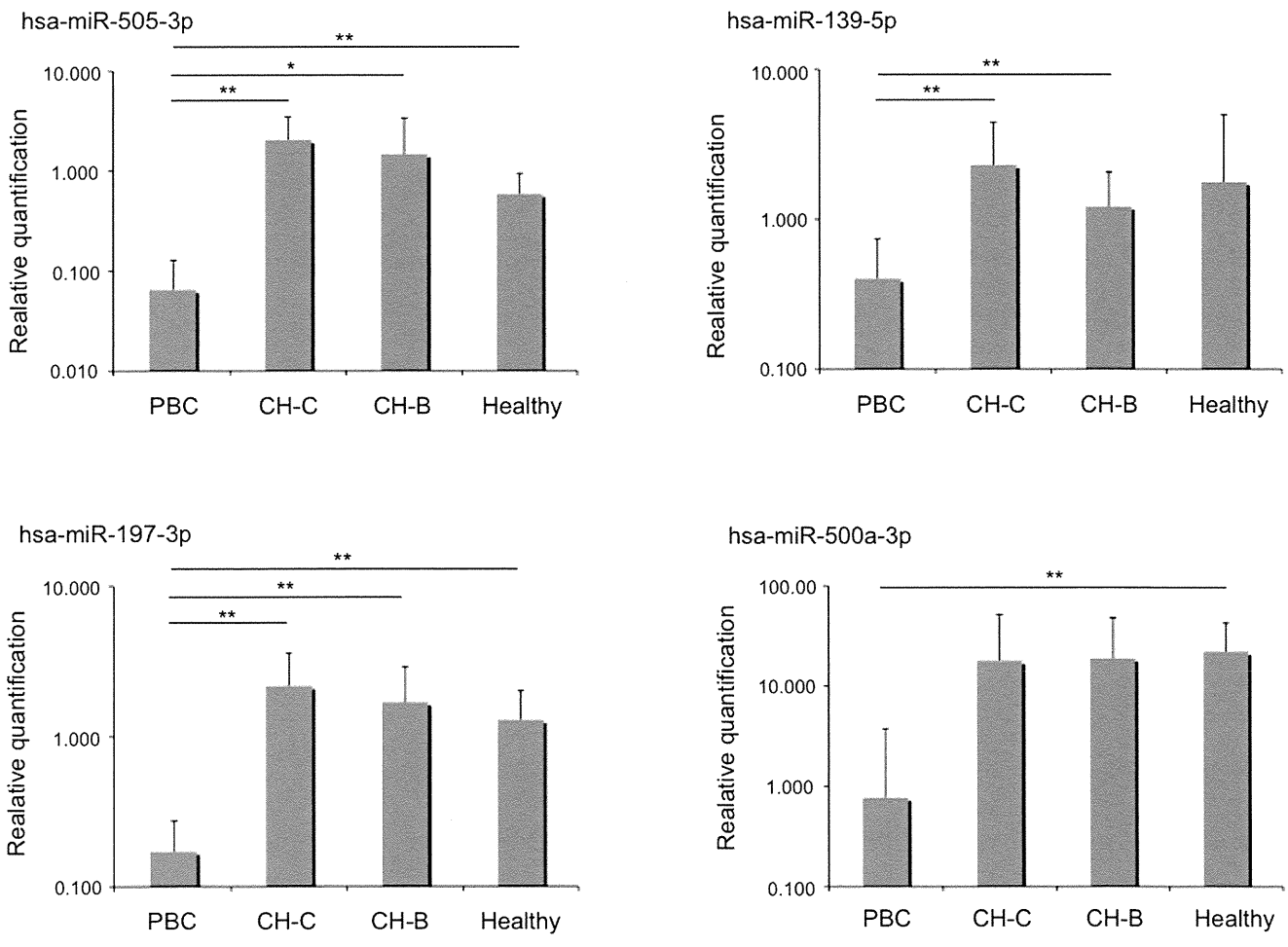

Figure 2. Validation of deep sequencing results for selected miRNAs. We have registered 10 samples in each group listed on Table S3. The threshold cycle for each miRNA primer/probe set were normalized with spiked in cel-miR-39 primer/probe pair and compared to CH-C-5. Result for normally distributed continuous variables are given as means and compared between groups by Student's t-test. Results for non-normally distributed continuous variables are summarized as medians and were compared by Mann-Whitney U test. Statistical significance indicates by one asterisk ($p<0.05$) and two ($p<0.01$).
doi:10.1371/journal.pone.0066086.g002

Table 5. Predicted target genes of 9 differentially expressed miRNA by Illumina sequencing in PBC.

Targets	Description	miRIS*	P-value
NM_000350	ATP-binding cassette, sub-family A (ABC1), member 4	0.250	1.83E-04
NM_000434	sialidase 1 (lysosomal sialidase) (NEU1), mRNA.	0.306	6.06E-04
NM_000491	complement component 1, q subcomponent, B chain	0.250	6.64E-04
NM_000663	4-aminobutyrate aminotransferase (ABAT), nuclear gene	0.417	9.55E-03
NM_000767	cytochrome P450, family 2, subfamily B, polypeptide 6	0.361	3.72E-03
NM_000878	interleukin 2 receptor, beta (IL2RB), mRNA.	0.250	7.10E-03
NM_001001716	nuclear factor of kappa light polypeptide gene	0.306	8.66E-03
NM_001007214	calcyclin binding protein (CACYBP), transcript variant	0.306	1.90E-03
NM_001012320	zinc finger protein 302 (ZNF302), transcript variant	0.306	3.32E-03
NM_001029997	zinc finger protein 181 (ZNF181), transcript variant	0.292	7.83E-03
NM_001033557	protein phosphatase 1B (formerly 2C),	0.250	7.51E-03
NM_001033910	TNF receptor-associated factor 5 (TRAF5), transcript	0.361	5.99E-03
NM_001034	ribonucleotide reductase M2 (RRM2), mRNA.	0.361	6.78E-03
NM_001098831	MORN repeat containing 4 (MORN4), transcript variant	0.306	4.68E-03
NM_001111125	IQ motif and Sec7 domain 2 (IQSEC2), transcript	0.361	2.49E-03
NM_001128932	cytochrome P450, family 4, subfamily F, polypeptide 11	0.361	8.47E-04
NM_001135146	solute carrier family 39 (zinc transporter), member 8	0.389	1.13E-03
NM_001136216	transmembrane protein 51 (TMEM51), transcript variant	0.250	2.75E-03
NM_001142289	mahogunin, ring finger 1 (MGRN1), transcript variant	0.361	7.27E-03
NM_001142353	protein phosphatase 3 (formerly 2B), catalytic	0.250	1.72E-03
NM_001142610	unc-51-like kinase 2 (C. elegans) (ULK2), transcript	0.347	5.97E-03
NM_001143944	LEM domain containing 2 (LEMD2), transcript variant 2,	0.250	2.08E-03
NM_001146699	RNA binding motif protein 19 (RBM19), transcript	0.306	6.81E-03
NM_001159322	phospholipase A2, group IVC (cytosolic,	0.292	1.32E-03
NM_001166	baculoviral IAP repeat-containing 2 (BIRC2), mRNA.	0.250	5.10E-03
NM_001293	chloride channel, nucleotide-sensitive, 1A (CLNS1A),	0.250	1.32E-03
NM_001337	chemokine (C-X3-C motif) receptor 1 (CX3CR1), mRNA.	0.417	1.39E-03
NM_001678	ATPase, Na+/K+ transporting, beta 2 polypeptide	0.417	4.07E-04
NM_001903	catenin (cadherin-associated protein), alpha 1, 102 kDa	0.389	3.97E-03
NM_002298	lymphocyte cytosolic protein 1 (L-plastin) (LCP1),	0.417	4.64E-03
NM_003810	tumor necrosis factor (ligand) superfamily, member 10	0.250	1.95E-03
NM_004414	regulator of calcineurin 1 (RCAN1), transcript variant	0.250	5.21E-03
NM_004642	cyclin-dependent kinase 2 associated protein 1	0.306	8.18E-04
NM_005046	kallikrein-related peptidase 7 (KLK7), transcript	0.306	7.63E-03
NM_005371	methyltransferase like 1 (METTL1), transcript variant	0.250	2.91E-03
NM_005517	high-mobility group nucleosomal binding domain 2	0.417	8.69E-03
NM_005736	ARP1 actin-related protein 1 homolog A, centractin	0.361	8.46E-03
NM_006598	solute carrier family 12 (potassium/chloride	0.361	5.04E-03
NM_014012	RAS (RAD and GEM)-like GTP-binding 1 (REM1), mRNA.	0.250	7.27E-03
NM_014452	tumor necrosis factor receptor superfamily, member 21	0.250	1.53E-03
NM_014567	breast cancer anti-estrogen resistance 1 (BCAR1),	0.250	6.32E-03
NM_014718	calsyntenin 3 (CLSTN3), mRNA.	0.250	3.78E-03
NM_014784	Rho guanine nucleotide exchange factor (GEF) 11	0.306	7.74E-03
NM_015278	SAM and SH3 domain containing 1 (SASH1), mRNA.	0.417	8.14E-03
NM_015352	protein O-fucosyltransferase 1 (POFUT1), transcript	0.472	1.47E-03
NM_016033	family with sequence similarity 82, member B (FAM82B),	0.458	3.43E-03
NM_016332	selenoprotein X, 1 (SEPX1), mRNA.	0.306	4.68E-03
NM_019072	small glutamine-rich tetratricopeptide repeat	0.417	8.71E-03
NM_019860	5-hydroxytryptamine (serotonin) receptor 7 (adenylate	0.250	7.39E-04

Table 5. Cont.

Targets	Description	miRIS*	P-value
NM_020211	RGM domain family, member A (RGMA), mRNA.	0.250	3.32E-03
NM_021131	protein phosphatase 2A activator, regulatory subunit 4	0.403	5.94E-03
NM_021939	FK506 binding protein 10, 65 kDa (FKBP10), mRNA.	0.306	1.13E-03
NM_021943	zinc finger, AN1-type domain 3 (ZFAND3), mRNA.	0.306	1.60E-03
NM_022497	mitochondrial ribosomal protein S25 (MRPS25), nuclear	0.417	8.60E-03
NM_024025	dual specificity phosphatase 26 (putative) (DUSP26),	0.403	1.66E-03
NM_024596	microcephalin 1 (MCPH1), mRNA.	0.361	1.00E-03
NM_024637	galactose-3-O-sulfotransferase 4 (GAL3ST4), mRNA.	0.361	1.73E-03
NM_024667	vacuolar protein sorting 37 homolog B (S. cerevisiae)	0.306	3.92E-03
NM_024898	DENN/MADD domain containing 1C (DENND1C), mRNA.	0.250	7.54E-03
NM_025108	chromosome 16 open reading frame 59 (C16orf59), mRNA.	0.250	3.39E-03
NM_031287	splicing factor 3b, subunit 5, 10kDa (SF3B5), mRNA.	0.306	4.48E-03
NM_032139	ankyrin repeat domain 27 (VPS9 domain) (ANKRD27),	0.306	9.38E-03
NM_032497	zinc finger protein 559 (ZNF559), mRNA.	0.347	4.45E-03
NM_080678	ubiquitin-conjugating enzyme E2F (putative) (UBE2F),	0.347	3.60E-03
NM_138396	membrane-associated ring finger (C3HC4) 9 (MARCH9),	0.306	5.18E-04
NM_138799	membrane bound O-acyltransferase domain containing 2	0.361	7.92E-03
NM_145168	short chain dehydrogenase/reductase family 42E, member	0.306	8.59E-03
NM_147202	chromosome 9 open reading frame 25 (C9orf25), mRNA.	0.417	4.67E-03
NM_173509	family with sequence similarity 163, member A	0.361	2.90E-03
NM_175839	spermine oxidase (SMOX), transcript variant 1, mRNA.	0.361	4.28E-03
NM_178468	family with sequence similarity 83, member C (FAM83C),	0.250	4.68E-03
NM_178832	MORN repeat containing 4 (MORN4), transcript variant	0.306	4.68E-03
NM_178835	zinc finger protein 827 (ZNF827), mRNA.	0.361	5.67E-03
NM_182527	calcium binding protein 7 (CABP7), mRNA.	0.417	1.95E-03
NM_198853	tripartite motif-containing 74 (TRIM74), mRNA.	0.403	1.82E-03

*miRIS :miRror Internal Score ranges from 0 top 1 by average 2 components (number of databases and input hits).

doi:10.1371/journal.pone.0066086.t005

gov/) [52]. DAVID can detect functional enrichment of a gene list based on the GO terms, KEGG pathway and BIOCARTA pathway. Differences were considered significant when the P value was less than 0.05.

Ethics statement

This study was approved by the Ethics Committee of the Tohoku University School of Medicine (2010-404) and written informed consent was obtained from each individual.

Supporting Information

Figure S1 The pathway of cell-to-cell adhesion signaling. The functional annotation analysis of BIOCARTA showed that the genes of catenin (cadherion-associated protein), alpha 1 and similar to breast cancer anti-estrogen resistance 1 played roles in this pathway. The stars indicate the related genes.
(TIFF)

Figure S2 The pathway of apoptosis. The functional annotation analysis of BIOCARTA showed that the genes of baculoviral IAP repeat-containing 2, protein phosphatase 3 (formerly 2B), catalytic subunit, beta isoform and tumor necrosis factor (ligand) superfamily, member 10 was related to apoptosis. The gene is indicated with the stars.
(TIFF)

Table S1 The list of differential expression levels of miRNA in each sample.
(XLS)

Table S2 Biological function analysis in GO terms of predicted gene targets of differentially regulated miRNAs using DAVID.
(DOC)

Acknowledgments

We thank M. Tsuda, M. Kikuchi, N. Koshita and K. Kuroda for technical assistance. We also acknowledge the support of the Biomedical Research Core of Tohoku University Graduate School of Medicine.

Accession number of DNA data bank of Japan (DDBJ) for the deep-sequence data reported in this paper is DRA000933.

Author Contributions

Conceived and designed the experiments: TS KN YU YK MN. Performed the experiments: MN RF. Analyzed the data: MN TN. Contributed reagents/materials/analysis tools: YK TK EK OK. Wrote the paper: MN YU.

References

1. Lau NC, Lim LP, Weinstein EG, Bartel DP (2001) An abundant class of tiny RNAs with probable regulatory roles in Caenorhabditis elegans. Science 294: 858–862.
2. Lagos-Quintana M, Rauhut R, Lendeckel W, Tuschl T (2001) Identification of novel genes coding for small expressed RNAs. Science 294: 853–858.
3. Lee RC, Ambros V (2001) An extensive class of small RNAs in Caenorhabditis elegans. Science 294: 862–864.
4. Bartel DP (2004) MicroRNAs: genomics, biogenesis, mechanism, and function. Cell 116: 281–297.
5. Chen X, Ba Y, Ma L, Cai X, Yin Y, et al. (2008) Characterization of microRNAs in serum: a novel class of biomarkers for diagnosis of cancer and other diseases. Cell Research 18: 997–1006.
6. Lu J, Getz G, Miska EA, Alvarez-Saavedra E, Lamb J, et al. (2005) MicroRNA expression profiles classify human cancers. Nature 435: 834–838.
7. Bihrer V, Friedrich-Rust M, Kronenberger B, Forestier N, Haupenthal J, et al. (2011) Serum miR-122 as a biomarker of necroinflammation in patients with chronic hepatitis C virus infection. Am J Gastroenterol 106: 1663–1669.
8. Zhang Y, Jia Y, Zheng R, Guo Y, Wang Y, et al. (2010) Plasma microRNA-122 as a biomarker for viral-, alcohol-, and chemical-related hepatic diseases. Clin Chem 56: 1830–1838.
9. Cermelli S, Ruggieri A, Marrero JA, Ioannou GN, Beretta L (2011) Circulating MicroRNAs in Patients with Chronic Hepatitis C and Non-Alcoholic Fatty Liver Disease. PLoS One 6: e23937.
10. Morita K, Taketomi A, Shirabe K, Umeda K, Kayashima H, et al. (2011) Clinical significance and potential of hepatic microRNA-122 expression in hepatitis C. Liver Int 31: 474–484.
11. Li LM, Hu ZB, Zhou ZX, Chen X, Liu FY, et al. (2010) Serum microRNA Profiles Serve as Novel Biomarkers for HBV Infection and Diagnosis of HBV-Positive Hepatocarcinoma. Cancer Research 70: 9798–9807.
12. Nakanuma Y, Ohta G (1979) Histometric and serial section observations of the intrahepatic bile ducts in primary biliary cirrhosis. Gastroenterology 76: 1326–1332.
13. Gershwin ME, Mackay IR, Sturgess A, Coppel RL (1987) Identification and specificity of a cDNA encoding the 70 kd mitochondrial antigen recognized in primary biliary cirrhosis. J Immunol 138: 3525–3531.
14. Coppel RL, McNeilage LJ, Surh CD, Van de Water J, Spithill TW, et al. (1988) Primary structure of the human M2 mitochondrial autoantigen of primary biliary cirrhosis: dihydrolipoamide acetyltransferase. Proc Natl Acad Sci U S A 85: 7317–7321.
15. Selmi C, Mayo MJ, Bach N, Ishibashi H, Invernizzi P, et al. (2004) Primary biliary cirrhosis in monozygotic and dizygotic twins: genetics, epigenetics, and environment. Gastroenterology 127: 485–492.
16. Begovich AB, Klitz W, Moonsamy PV, Van de Water J, Peltz G, et al. (1994) Genes within the HLA class II region confer both predisposition and resistance to primary biliary cirrhosis. Tissue Antigens 43: 71–77.
17. Donaldson PT, Baragiotta A, Heneghan MA, Floreani A, Venturi C, et al. (2006) HLA class II alleles, genotypes, haplotypes, and amino acids in primary biliary cirrhosis: a large-scale study. Hepatology 44: 667–674.
18. Onishi S, Sakamaki T, Maeda T, Iwamura S, Tomita A, et al. (1994) DNA typing of HLA class II genes; DRB1*0803 increases the susceptibility of Japanese to primary biliary cirrhosis. J Hepatol 21: 1053–1060.
19. Hirschfield GM, Liu X, Xu C, Lu Y, Xie G, et al. (2009) Primary biliary cirrhosis associated with HLA, IL12A, and IL12RB2 variants. N Engl J Med 360: 2544–2555.
20. Mells GF, Floyd JA, Morley KI, Cordell HJ, Franklin CS, et al. (2011) Genome-wide association study identifies 12 new susceptibility loci for primary biliary cirrhosis. Nat Genet 43: 329–332.
21. Hirschfield G, Invernizzi P (2011) Progress in the Genetics of Primary Biliary Cirrhosis. Seminars in Liver Disease 31: 147–156.
22. Nakamura M, Nishida N, Kawashima M, Aiba Y, Tanaka A, et al. (2012) Genome-wide Association Study Identifies TNFSF15 and POU2AF1 as Susceptibility Loci for Primary Biliary Cirrhosis in the Japanese Population. Am J Hum Genet 91: 721–728.
23. Lindor KD, Gershwin ME, Poupon R, Kaplan M, Bergasa NV, et al. (2009) Primary biliary cirrhosis. Hepatology 50: 291–308.
24. Corpechot C, Poupon R (2007) Geotherapeutics of primary biliary cirrhosis: Bright and sunny around the Mediterranean but still cloudy and foggy in the United Kingdom. Hepatology 46: 963–965.
25. Metcalf JV, Mitchison HC, Palmer JM, Jones DE, Bassendine MF, et al. (1996) Natural history of early primary biliary cirrhosis. Lancet 348: 1399–1402.
26. Gilad S, Meiri E, Yogev Y, Benjamin S, Lebanony D, et al. (2008) Serum microRNAs are promising novel biomarkers. PLoS One 3: e3148.
27. Martin M (2011) Cutadapt removes adapter sequences from high-throughput sequencing reads. EMBnet journal 17: 10–12.
28. Robinson MD, Oshlack A (2010) A scaling normalization method for differential expression analysis of RNA-seq data. Genome Biology 11: R25.
29. Balaga O, Friedman Y, Linial M (2012) Toward a combinatorial nature of microRNA regulation in human cells. Nucleic Acids Res 40: 9404–9416.
30. Juran BD, Lazaridis KN (2010) Update on the genetics and genomics of PBC. J Autoimmun 35: 181–187.
31. Zhang R, Peng Y, Wang W, Su B (2007) Rapid evolution of an X-linked microRNA cluster in primates. Genome Res 17: 612–617.
32. Mitchell PS, Parkin RK, Kroh EM, Fritz BR, Wyman SK, et al. (2008) Circulating microRNAs as stable blood-based markers for cancer detection. Proceedings of the National Academy of Sciences 105: 10513–10518.
33. Ai J, Zhang R, Li Y, Pu J, Lu Y, et al. (2010) Circulating microRNA-1 as a potential novel biomarker for acute myocardial infarction. Biochemical and Biophysical Research Communications 391: 73–77.
34. Chim SSC, Shing TKF, Hung ECW, Leung Ty, Lau Tk, et al. (2008) Detection and Characterization of Placental MicroRNAs in Maternal Plasma. Clinical Chemistry 54: 482–490.
35. Starkey Lewis PJ, Dear J, Platt V, Simpson KJ, Craig DGN, et al. (2011) Circulating microRNAs as potential markers of human drug-induced liver injury. Hepatology 54: 1767–1776.
36. Wang K, Zhang S, Marzolf B, Troisch P, Brightman A, et al. (2009) Circulating microRNAs, potential biomarkers for drug-induced liver injury. Proceedings of the National Academy of Sciences 106: 4402–4407.
37. Tsujiura M, Ichikawa D, Komatsu S, Shiozaki A, Takeshita H, et al. (2010) Circulating microRNAs in plasma of patients with gastric cancers. British Journal of Cancer 102: 1174–1179.
38. Kong X, Du Y, Wang G, Gao J, Gong Y, et al. (2010) Detection of Differentially Expressed microRNAs in Serum of Pancreatic Ductal Adenocarcinoma Patients: miR-196a Could Be a Potential Marker for Poor Prognosis. Digestive Diseases and Sciences 56: 602–609.
39. Silva J, Garcia V, Zaballos A, Provencio M, Lombardia L, et al. (2010) Vesicle-related microRNAs in plasma of nonsmall cell lung cancer patients and correlation with survival. European Respiratory Journal 37: 617–623.
40. Li M, Marin-Muller C, Bharadwaj U, Chow K-H, Yao Q, et al. (2008) MicroRNAs: Control and Loss of Control in Human Physiology and Disease. World Journal of Surgery 33: 667–684.
41. Berg CP, Stein GM, Keppeler H, Gregor M, Wesselborg S, et al. (2007) Apoptosis-associated antigens recognized by autoantibodies in patients with the autoimmune liver disease primary biliary cirrhosis. Apoptosis 13: 63–75.
42. Liang Y, Yang Z, Li C, Zhu Y, Zhang L, et al. (2008) Characterisation of TNF-related apoptosis-inducing ligand in peripheral blood in patients with primary biliary cirrhosis. Clinical and Experimental Medicine 8: 1–7.
43. Ashburner M, Ball CA, Blake JA, Botstein D, Butler H, et al. (2000) Gene ontology: tool for the unification of biology. The Gene Ontology Consortium. Nat Genet 25: 25–29.
44. Nakagome Y, Ueno Y, Kogure T, Fukushima K, Moritoki Y, et al. (2007) Autoimmune cholangitis in NOD.c3c4 mice is associated with cholangiocyte-specific Fas antigen deficiency. J Autoimmun 29: 20–29.
45. Singh R, Bullard J, Kalra M, Assefa S, Kaul AK, et al. (2011) Status of bacterial colonization, Toll-like receptor expression and nuclear factor-kappa B activation in normal and diseased human livers. Clinical Immunology 138: 41–49.
46. Kyriakou DS, Alexandrakis MG, Zachou K, Passam F, Stathakis NE, et al. (2003) Hemopoietic progenitor cells and bone marrow stromal cells in patients with autoimmune hepatitis type 1 and primary biliary cirrhosis. J Hepatol 39: 679–685.
47. Maglott D, Ostell J, Pruitt KD, Tatusova T (2010) Entrez Gene: gene-centered information at NCBI. Nucleic Acids Research 39: D52–D57.
48. Kozomara A, Griffiths-Jones S (2010) miRBase: integrating microRNA annotation and deep-sequencing data. Nucleic Acids Research 39: D152–D157.
49. Benjamini Y, Hochberg Y (1995) Controlling the false discovery rate: A practical and powerful approach to multiple testing. Journal of the Royal Statistical Society 57: 289–300.
50. Team RDC (2011) R: a language and environment for statistical computing. Vienna, Austria: the R Foundation for Statistical Computing.
51. Friedman Y, Naamati G, Linial M (2010) MiRror: a combinatorial analysis web tool for ensembles of microRNAs and their targets. Bioinformatics 26: 1920–1921.
52. Dennis G, Jr., Sherman BT, Hosack DA, Yang J, Gao W, et al. (2003) DAVID: Database for Annotation, Visualization, and Integrated Discovery. Genome Biol 4: P3.
53. Knodell RG, Ishak KG, Black WC, Chen TS, Craig R, et al. (1981) Formulation and application of a numerical scoring system for assessing histological activity in asymptomatic chronic active hepatitis. Hepatology 1: 431–435.
54. Ludwig J, Dickson ER, McDonald GS (1978) Staging of chronic nonsuppurative destructive cholangitis (syndrome of primary biliary cirrhosis). Virchows Arch A Pathol Anat Histol 379: 103–112.
55. Scheuer P (1967) Primary biliary cirrhosis. Proceedings of the Royal Society of Medicine 60: 1257–1260.
56. Ward JH (1963) Hierarchical Grouping to Optimize an Objective Function. Journal of the American Statistical Association 58: 236–244.

Y Chromosome–Linked B and NK Cell Deficiency in Mice

Shu-lan Sun,* Satoshi Horino,* Ari Itoh-Nakadai,† Takeshi Kawabe,* Atsuko Asao,* Takeshi Takahashi,‡ Takanori So,* Ryo Funayama,§ Motonari Kondo,¶ Hirotomo Saitsu,‖ Naomichi Matsumoto,‖ Keiko Nakayama,§ and Naoto Ishii*

There are no primary immunodeficiency diseases linked to the Y chromosome, because the Y chromosome does not contain any vital genes. We have established a novel mouse strain in which all males lack B and NK cells and have Peyer's patch defects. By 10 wk of age, 100% of the males had evident immunodeficiencies. Mating these immunodeficient males with wild-type females on two different genetic backgrounds for several generations demonstrated that the immunodeficiency is linked to the Y chromosome and is inherited in a Mendelian fashion. Although multicolor fluorescence in situ hybridization analysis showed that the Y chromosome in the mutant male mice was one third shorter than that in wild-type males, exome sequencing did not identify any significant gene mutations. The precise molecular mechanisms are still unknown. Bone marrow chimeric analyses demonstrated that an intrinsic abnormality in bone marrow hematopoietic cells causes the B and NK cell defects. Interestingly, fetal liver cells transplanted from the mutant male mice reconstituted B and NK cells in lymphocyte-deficient *Il2rg*$^{-/-}$ recipient mice, whereas adult bone marrow transplants did not. Transducing the EBF gene, a master transcription factor for B cell development, into mutant hematopoietic progenitor cells rescued B cell but not NK cell development both in vitro and in vivo. These Y chromosome–linked immunodeficient mice, which have preferential B and NK cell defects, may be a useful model of lymphocyte development.
***The Journal of Immunology*, 2013, 190: 6209–6220.**

Most primary immunodeficiencies are inherited disorders. For example, mutations of the common cytokine receptor γ-chain *(Il2rg)* gene, which is located on the X chromosome, cause X-linked SCID, which is characterized by T and NK cell deficiencies and functionally impaired mature B cells. Mutations of the recombinase-activating genes *Rag1* and *Rag2* induce T and B cell deficiencies while retaining functional NK cells. These immunodeficiencies are caused by gene mutations on an autosome or an X chromosome (1, 2). No hereditary Y chromosome–linked immunodeficiencies have been reported in humans.

The Y chromosome is one of two chromosomes that pair with the X chromosome and determine sex in most mammals. The mouse Y chromosome is 16-Mb long and contains 54 genes; the human Y chromosome is 58-Mb long and encodes 86 genes. It is apparent that Y chromosomes do not contain genes essential for life, because females do not have the Y chromosome. Only two studies showed the male mice–specific disorder that is Y chromosome linked. One is Yaa (Y-linked autoimmune accelerator). Yaa mice develop a disease similar to systemic lupus erythematosus, and the incidence and onset are much higher in males than in their female littermates in certain mouse strains, including BXSB and MLR (3). Recent studies have shown that in Yaa mice, the part of the X chromosome pseudoautosomal region containing the *TLR7* gene is translocated onto the Y chromosome. Therefore, the duplication of TLR7, which may render B cells hypersensitive to self-Ags containing RNA, contributes to the BXSB strain's Y-linked autoimmune-prone phenotype. However, the *Yaa* mutation alone is not sufficient to induce autoimmune disease in C56BL/6 male mice; additional genetic mutations are required. In this context, the autoimmune disease associated with the *Yaa* mutation is not a Y-chromosomal Mendelian disease. Another study showed a mouse strain in which Vα14i NKT cell is absent in the male mice (4). However, they did not analyze the Y chromosome, so the mechanism of Y chromosome–linked NKT deficiency is still unknown.

B cells are lymphocytes that play a large role in humoral immune responses. Murine B cell development is initiated in the fetal liver cells and relocates to the bone marrow after birth. B cell development requires the coordinated efforts of transcription factors and cytokines, particularly IL-7 (5). IL-7 regulates early B cell transcription factor (EBF) expression in the adult bone marrow (6). EBF is a B cell–specific transcription factor that regulates crucial genes affecting B cell development, such as *λ5*, *Vpre B*, and *mb-1* (7, 8). EBF cooperates with E2A to positively regulate Pax5 expression. These transcription factors, along with PU.1, are indispensable for B cell development (9–11).

NK cells are a distinct lymphocyte subset with a central role in innate immunity (12). Early studies suggested that NK cells, like B cells and myeloid-lineage cells, develop primarily in the bone marrow. NK precursor (NKP) cells derived from hematopoietic stem cells (HSCs) give rise to immature NK (iNK) and then

*Department of Microbiology and Immunology, Tohoku University Graduate School of Medicine, Sendai 980-8575, Japan; †Department of Biochemistry, Tohoku University Graduate School of Medicine, Sendai 980-8575, Japan; ‡Central Institute for Experimental Animals, Kawasaki 210-0821, Japan; §Department of Cell Proliferation, Tohoku University Graduate School of Medicine, Sendai 980-8575, Japan; ¶Department of Immunology, Toho University School of Medicine, Tokyo 143-8540, Japan; and ‖Department of Human Genetics, Yokohama City University Graduate School of Medicine, Yokohama 236-0004, Japan

Received for publication January 31, 2013. Accepted for publication April 19, 2013.

This work was supported in part by a grant-in-aid for scientific research on priority areas from the Ministry of Education, Science, Sports and Culture of Japan, a grant-in-aid for scientific research on priority areas from the Japan Society for the Promotion of Science, and grants from the Japan Science and Technology Agency, the Sumitomo Foundation, the Uehara Memorial Foundation, the Novartis Foundation for the Promotion of Science, and the Yakult Bio-Science Foundation.

Address correspondence and reprint requests to Prof. Naoto Ishii, Department of Microbiology and Immunology, Tohoku University Graduate School of Medicine, 2-1 Seiryo-machi, Aoba-ku, Sendai 980-8575, Japan. E-mail address: ishiin@med.tohoku.ac.jp

Abbreviations used in this article: E, embryonic day; EBF, early B cell transcription factor; FISH, fluorescence in situ hybridization; HPC, hematopoietic progenitor cell; iNK, immature NK; NKP, NK precursor; PP, Peyer's patch; SCF, stem cell factor.

www.jimmunol.org/cgi/doi/10.4049/jimmunol.1300303

mature NK cells. Several transcription factors, such as Ets-1, Id2, PU.1, Ikaros, T-bet, E4BP4, and Irf-2 are required for NK cell maturation (12–14). Among these, PU.1, Ikaros, and Ets-1 are critical for generating NKPs, and the other factors become involved after cells are committed to the NK cell lineage. For example, *Id2*$^{-/-}$ mice have normal numbers of NKP and iNK cells but significantly fewer mature NK cells (15). However, these factors are not necessarily specific to the NK lineage, because their individual deletions sometimes cause defects in other hematopoietic cell lineages.

In this study, we established a novel immunodeficient mouse strain characterized by Y chromosome–linked hereditary B and NK cell deficiencies. B and NK cells gradually diminished after 3 wk of age and disappeared by 10 wk of age in 100% of the males of this strain. B cell development was arrested at the prepro-B cell stage, and NKP cells were almost undetectable in these mutant mice. Although intensive genomic analyses failed to reveal the precise molecular mechanisms of this Y-linked lymphocyte deficiency, the mouse phenotype suggests that a mutation of one gene may cause B and NK cell deficiency without affecting T cell development. Therefore, this novel mouse strain may be a useful model for distinguishing the developmental processes of B, T, and NK cells, which are thought to derive from common lymphoid progenitor cells.

Materials and Methods

Mice

B cell–deficient mice on a C57BL/6N background were bred and maintained under specific pathogen-free conditions. Unless otherwise indicated, age-matched (3–20 wk old) and female littermates were used as controls. All procedures were performed according to protocols approved by Tohoku University's Institutional Committee for the Use and Care of Laboratory Animals.

Flow cytometry

Single-cell suspensions were prepared and cells immunostained as previously described (16). Dead cells were positively stained by propidium iodide and excluded from analysis. Lymphocyte suspensions from the spleen, bone marrow, peripheral blood, and fetal liver were incubated with a CD16/32 mAb (2.4G2) and stained for 30 min on ice with a combination of the following mouse-specific Abs: FITC-CD19 (6D5; BioLegend, San Diego, CA), PE–anti-IgM (eB121-15F9; eBioscience, San Diego, CA), PE-CD3 (eBio500A2; eBioscience), Pacific Blue-CD4 (RM4-5; BD Pharmingen, San Diego, CA), allophycocyanin-CD8 (53-6.7; BioLegend), FITC-CD11b (M1/70; BD Pharmingen), PE–anti-NK1.1 (PK136; BD Pharmingen), allophycocyanin–anti-B220 (RA3-6B2; BioLegend), FITC-CD90.2 (53-2.1; BD Pharmingen), FITC-CD43 (S7; BD Pharmingen), PE–anti-Ly5.1 (6c3; BioLegend), Pacific Blue-CD24 (M1/69; BioLegend), FITC-CD34 (RAM34; BD Pharmingen), allophycocyanin-CD117 (2B8; BioLegend), PE/Cy7–anti-Sca-1 (D7; BioLegend), Biotin-CD127 (A7R34; BioLegend), Biotin-CD122 (TM-β1; BioLegend), PE-CD5 (53-7.3; BD Pharmingen), FITC–Gr-1 (RB6-8C5; BD Pharmingen), PE-Ter119 (TER119; BioLegend), FITC-CD71 (RI7217; BioLegend), allophycocyanin-CD3 (145-2c11; BioLegend), and PE–anti-IgM (eB121-15F9; eBioscience). Biotinylated Abs were visualized by BD Horizon V450 streptavidin (BD Pharmingen). Samples were analyzed with an FACSCanto II or LSRFortessa system (BD Biosciences); data were analyzed with FlowJo flow cytometry analysis software (Tree Star).

Radioactive proliferation assay

Splenic T cells were first separated by CD90.2 Microbeads (Miltenyi Biotec, Bergisch Gladbach, Germany). A total of 1×10^5 cells was then seeded in the wells of a 96-well plate precoated with 10 μg/ml anti-mouse CD3e mAb (145-2C11) in a RPMI 1640 containing 10% FCS, 200 U/ml streptomycin, 200 U/ml penicillin, 50 μM 2-ME, and 1 μg/ml anti-mouse CD28 mAb. After 48 h stimulation, 1 μCi/well [^{3}H]thymidine was added, and the incorporation of [^{3}H]thymidine was measured by a γ-scintillation counter.

Real-time PCR

Prepro-B ($B220^+CD43^-CD24^-Ly51^-$) cells were purified from bone marrow cells using an FACSAria II cell sorter (BD Biosciences) and lysed with 1 ml TRIzol reagent (Invitrogen, Carlsbad, CA). Total RNA was purified from the cells. The cDNA was then synthesized with SuperScript Reverse Transcriptase and Random Primers (Invitrogen). The cDNA was then amplified over 40 cycles on a 7500 Real-time PCR system using SYBR Premix EXtaq (TaKaRa Bio, Shiga, Japan), ROX Reference DyeII (TaKaRa Bio), and primer sets. All samples were normalized to GAPDH. The PCR primers for E12, E47, EBF, PU.1, Id2, Ikaros, and GAPDH were as follows: E12 forward, 5′-GGGAGGAGAAAGAGGATGA-3′ and reverse, 5′-GCTCCGCCTTCTGCTCTG-3′; E47 forward, 5′-GGGAGGAGAAAGAGGATGA-3′ and reverse, 5′-CCGGTCCCTCAGGTCCTTC-3′; PU.1 forward, 5′-GAACAGATGCACGTCCTCGAT-3′ and reverse, 5′-GGGGACAAGGTTTGATAAGGGAA-3′; EBF forward, 5′-CTACAGCAATGGGATACGGAC-3′; reverse, 5′-TTTCAGGGTTCTTGTCTTGGC-3′; Id2 forward, 5′-CTCCAAGCTCAAGGAACTGG-3′ and reverse, 5′-ATTCAGATGCCTGCAAGGAC-3′; Ikaros forward, 5′-TGTGTCATCGGAGCGAGAG-3′ and reverse, 5′-GGAAGGCATCCTGCGAGTT-3′; and GAPDH forward, 5′-CCAGGTTGTCTCCTGCGACTT-3′ and reverse, 5′-CCTGTTGCTGTAGCCGTATTCA-3′.

Adoptive cell transfer

Bone marrow cells were extracted by a pressurized flow of sterile tissue-culture medium through femurs and tibias dissected from donor mice. Fetal liver cells were taken from female or male mice at embryonic day (E) 17.5. Recipient *Il2rg*$^{-/-}$ mice were irradiated with 5 Gy, and on the following day, 4×10^6 adult bone marrow cells or fetal liver cells were transplanted into recipients via the tail vein.

Purification of hematopoietic progenitor cells from bone marrow and fetal liver

Hematopoietic progenitor cells (HPCs) were purified from adult bone marrow or E17.5 fetal liver cells by staining with the following mouse-specific, biotinylated lineage markers: CD3, B220, TER119, Gr1, DX5, and CD11b. HPCs were negatively separated by anti-Biotin MicroBeads with auto MACS Columns (Miltenyi Biotec).

In vitro lymphopoiesis

HPCs collected from adult bone marrow or E17.5 fetal liver cells were cultured on OP9 stromal cells in α-MEM medium containing 20% FCS, 200 U/ml streptomycin, 200 U/ml penicillin, and 50 μM 2-ME or 7 d. For B cell development, the medium was supplemented with 5 ng/ml stem cell factor (SCF), 5 ng/ml Flt3 ligand, and 10 ng/ml IL-7; for NK cells, the medium was supplemented with 5 ng/ml SCF, 5 ng/ml Flt3 ligand, and 30 ng/ml IL-15.

Retroviral transduction

We produced a virus from a packaging cell line, PLAT-E, by transiently transfecting the MSCV-EBF-IRES-GFP plasmid (6) and MSCV-IRES-GFP as control using FuGENE transfection reagent (Roche, Madison, WI). HPCs from males (Ly5.2) or female littermates (Ly5.2) were cultured in RPMI 1640 containing 10% FCS, 200 U/ml streptomycin, 200 U/ml penicillin, and 50 μM 2-ME supplemented with mouse recombinant SCF (50 ng/ml), IL-6 (10 ng/ml), IL-3 (5ng/ml), FLT-3 ligand (5 ng/ml), and IL-7 (5 ng/ml). On the following day, the cells were transferred onto a RetroNectin-coated (TaKaRa Bio) plate in the presence of retroviral supernatant. For spin infection, the plate was centrifuged at $2000 \times g$ at 32°C for 2 h once daily on days 1 and 2. Two days postinfection, the cells were washed and then transferred into irradiated Ly5.1 wild-type mice or cocultured on OP9 cells under B or NK cell differentiation conditions.

Statistical analysis

Statistical analysis was performed by Student *t* test. The p values < 0.05 were considered significant.

Results

Mutant male mice lack NK and B cells and Peyer's patches

In our mouse population, a novel mutant strain emerged spontaneously, in which all males lacked Peyer's patches (PP) and mated these males with wild-type female mice, we observed their offspring for the presence or absence of PPs. Although PPs in both the male and female offspring were visible from 4 to 6 wk after birth, PPs were completely lacking in the male offspring as they grew up to 10 wk old (Fig. 1A and data not shown). This indicated

that the early PP compartmentalization process was normal in the male mice. Moreover, each male mouse had a normal number of lymph nodes, although the lymph nodes were abnormally small, and was outwardly normal in behavior, fertility, and appearance. To understand the characteristic of these mutant male mice, we analyzed hematopoietic cells in the spleen, peritoneal cavity, thymus, bone marrow, and peripheral blood. Interestingly, the males had virtually no B (B1 and B2) cells and also had significantly fewer NK cells ($NK1.1^+CD3^-$) than their female littermates (Fig. 1B, 1C). NK deficiency was also confirmed with a different NK cell marker ($CD3^-DX5^+FcR\varepsilon I^-$) (data not shown). However, there were no differences in the absolute cell number of myeloid and erythroid populations in the bone marrow or of RBCs in the periphery (Fig. 1B, 1F, 1G). In addition, the absolute

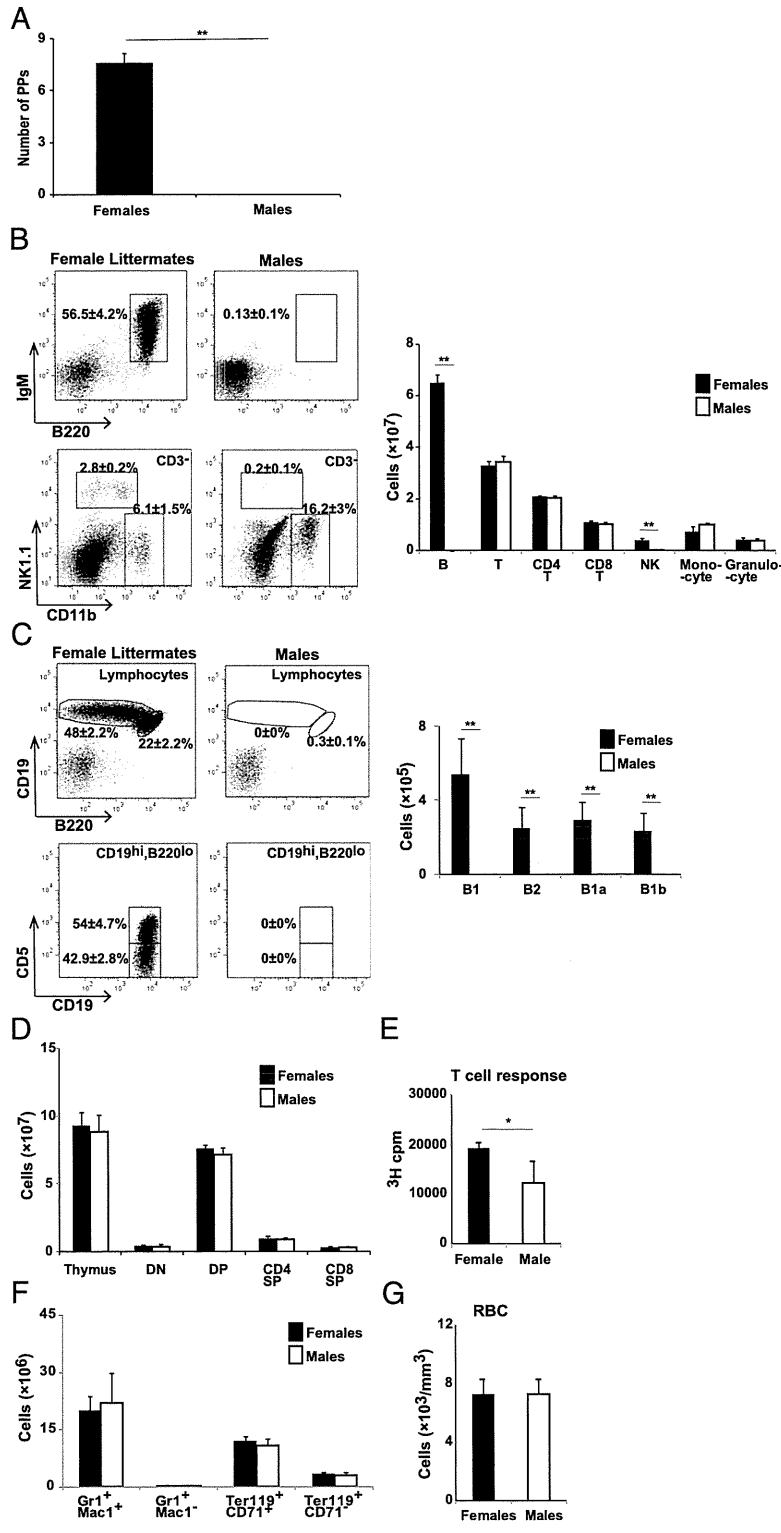

FIGURE 1. Mutant male mice specifically lack PPs. (**A**) Number of PPs on small intestines of 12-wk-old males or their female littermates. Frequency and the absolute number of hematopoietic lineages in the spleen (**B**), peritoneal cavity (**C**), thymus (**D**), and bone marrow (**F**) were analyzed by flow cytometry. $B220^+IgM^+$ B cell, $CD3^+$ T cell, $CD3^+CD4^+$ T cell, $CD3^+CD8^+$ T cell, $NK1.1^+CD3^-$ NK cell, $CD11b^+$ monocyte, and Gr-1^+ granulocyte populations are shown. (C) Peritoneal lymphocytes were separated into the following subsets: total B1, $CD19^+B220^{lo\text{-}int}$; B1a, $CD19^+B220^{lo\text{-}int}$ $D5^+$; and B1b, $CD19^+B220^{lo\text{-}int}$ $CD5^{lo/-}$. (D) Thymic cells were stained with CD4 and CD8 and separated into the following subsets: double-negative (DN), $CD4^-CD8^-$; double-positive (DP), $CD4^+CD8^+$; CD4 single-positive (SP), $CD4^+CD8^-$; and CD8 SP, $CD4^-CD8^+$. (**E**) Splenic T cells were stimulated with anti-CD3 and anti-CD28 mAbs for 4–8 h and then pulsed with [^{3}H]thymidine. The incorporation of [^{3}H]thymidine was measured. (F) Myeloid cells ($Gr1^+Mac1^+$ and $Gr1^+Mac1^-$), $Ter119^+CD71^+$ nucleated erythroid progenitors, and $Ter119^+$ $D71^-$ nonnucleated erythroid cells in the bone marrow were counted. (**G**) RBCs in the peripheral blood were counted. Numbers in FACS plots indicate the percentages relative to the gated cells. Data are from more than five experiments (A–D) or one experiment (E–G) with at least four mice per genotype. Error bars indicate SD (± SD). $*p < 0.05$, $**p < 0.01$.

number of T cell subsets in the thymus and spleen was comparable between the mutant males and the female littermate controls (Fig. 1B, 1D), suggesting normal T cell development in the mutant male mice. When splenic T cells were stimulated with anti-CD3ε mAb, the proliferative responses of T cells in the mutant male mice were clearly observed but significantly lower than female controls' (Fig. 1E).

B and NK cell deficiency is inherited in a Mendelian, Y chromosome–linked fashion

Because all male pups in this strain were B and NK cell deficient, we hypothesized that the phenotype might be inherited as a dominant trait linked to the Y chromosome. To confirm this, we mated PP (B and NK cell)–deficient male mice with wild-type female mice on a C57BL/6 (Fig. 2A, *left panel*) or BALB/c (Fig. 2A, *right panel*) background, and looked for PPs (B and NK cell) in their 10-wk-old offspring. All male offspring of a mutant male parent also lacked PPs (B and NK cells). In contrast, there was no abnormality in PPs or B cells in the female offspring or in males that inherited their Y chromosome from a wild-type male. The family tree indicated that the B and NK cell deficiency was inherited in a Mendelian fashion linked to the Y chromosome.

To determine the Y chromosome's genetic abnormality, we examined it by fluorescence in situ hybridization (FISH) analysis. The Y chromosome in the mutant males (n = 10) was one third shorter than that in wild-type male mice, suggesting a structural abnormality (Fig. 2B).

The Yaa mutation, which contributes to a higher incidence of autoimmune disease in male than in female BXSB mice, is caused by the novel translocation of a gene locus from the X chromosome onto the Y chromosome, resulting in the duplication of several genes. To look for duplication or copy-number abnormalities of certain genes in our B and NK cell–deficient male mice, we performed array-based comparative genomic hybridization with spleen cells and hepatic cells from mutant male and wild-type male mice on the same genetic background. We found gene-copy abnormalities of three autosomal gene loci (data not shown). However, FISH analysis with bacterial artificial chromosome clone probes derived from these three autosomal gene loci failed to find any evidence of an insertion or translocation of the loci into the Y chromosome (data not shown).

We also sequenced Y chromosome exomes from B and NK cell–deficient and wild-type male mice (n = 3 each) from the same B6 strain. However, we could not find any significant nucleotide differences, including single nucleotide polymorphisms, between the Y chromosome exons in mutant and wild-type mice (data not shown). Thus, the genetic Y chromosome abnormality responsible for the Y chromosome–linked immunodeficiency remains unclear.

B and NK cell populations in the mutant male mice decrease with age

B and NK cells were absent in the adult male mice of this strain. To examine whether B or NK cell lymphopenia occurs at birth, we measured the numbers of B and NK cells in the bone marrow, spleen, lymph nodes, and peripheral blood at 3, 6, 8, and 12 wk of age. The B and NK cell populations in males at 3 wk of age were comparable with those in females, but had decreased to a markedly lower level at 6 wk of age (Fig. 3A). Interestingly, B1 cells in the males were markedly reduced compared with those in the female littermates even at 3 wk after birth and completely disappeared by 12 wk of age (Fig. 3B). Consistent with B cell decline, serum IgG and IgM dramatically decreased at 6 wk of age (Fig. 3D). In contrast, T cells increased with age in both males and females and

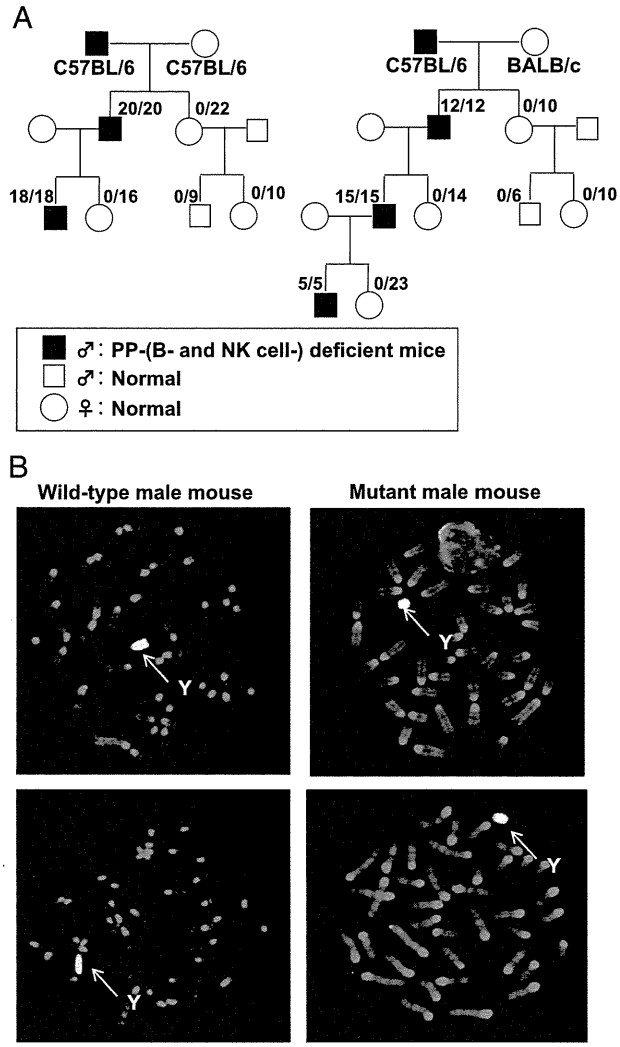

FIGURE 2. B and NK cell deficiency is inherited in a Mendelian fashion linked to the Y chromosome. (**A**) B cell–deficient male mice were mated with C57BL/6 (*left panel*) or BABL/c (*right panel*) wild-type female mice for several generations. The 10-wk-old offspring were then examined for B and NK cells in the peripheral blood and for PPs. Mice deficient in PPs (B and NK cells) are represented by filled symbols and unaffected individuals by open symbols (squares, males; circles, females). The numbers of immunodeficient mice/number of offspring are shown. (**B**) Y chromosomes from wild-type and B and NK cell–deficient males were analyzed by FISH. The Y chromosome is presented in yellow; pictures show Y chromosomes from different cells. Representative results are shown (n = 20 cells each).

the thymic development of T cells in the males was normal (Fig. 3A, 3C).

To rule out the possibility that androgenic hormones were associated with this phenotype, we compared splenic B and T cells in 10-wk-old B cell–deficient males that had been either castrated or subjected to a sham operation at 2 wk of age (Fig. 3D). The castrated male mice lacked B cells but had normal T cells, indicating that the male-specific B cell defect was independent of androgen.

Bone marrow lymphopoiesis in the mutant male mice is arrested at the prepro-B to pro-B cell transition

Because B cells were depleted in the adult male mutant mice, we looked at various stages of B cell differentiation to determine which stage was arrested. The B cell development from HSCs is sub-

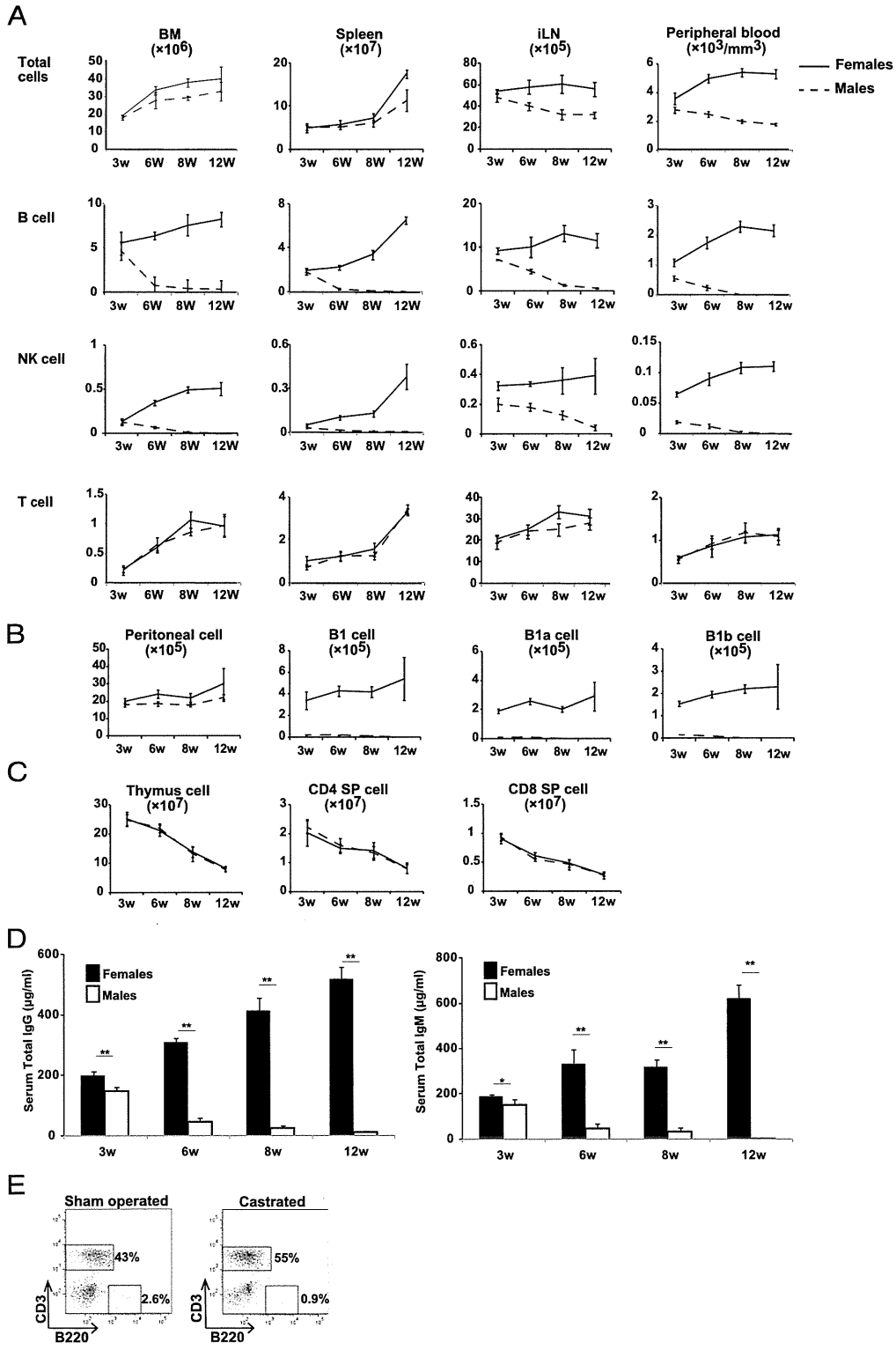

FIGURE 3. B and NK cell deficiencies are restricted to adults and are not affected by androgens. (**A**) Number of B cells ($B220^+$), T cells ($CD3^+$), and NK cells ($NK1.1^+$ $CD3^-$) from the bone marrow, spleen, inguinal lymph nodes (iLN), and blood. Numbers of B cell subsets in the peritoneal cavity (**B**) and number of T cell subset in the thymus (**C**) of male and female littermates at 3, 6, 8, and 12 wk of age. (**D**) Serum levels of IgG and IgM in 3-, 6-, 8-, and 12-wk-old mice were calculated from absorbance at 450 nm (A_{450}). Data are from one experiment ($n = 4$ mice/genotype). Error bars indicate SD (± SD). (**E**) The 2-wk-old male offspring of B cell–deficient male mice were castrated or subjected to a sham operation, and then the percentages of B and T cells in the spleen were compared at 10 wk of age. Data are from one experiment ($n = 2$ mice/group). $*p < 0.05$, $**p < 0.01$.

divided into Hardy fractions A–F (17). We found decreased numbers of B cell progenitors in the bone marrow that had undergone the transition from prepro-B to pro-B cells, corresponding to the Hardy fractions A ($B220^+CD43^+BP\text{-}1^-CD24^-$) and B ($B220^+CD43^+BP\text{-}1^-CD24^+$). Immature B cells, corresponding to Hardy fraction E ($B220^+CD43^-IgM^-IgD^+$), were severely deficient (Fig. 4A, 4B).

NK cells are lost in the mutant male mice

NK cells, which develop primarily in the bone marrow, are derived from HSCs via NKP and iNK cells. Because the very low number of splenic NKs in the mutant males suggested defective NK development, we compared the number of NKP and iNK cells in the bone marrow of males and their female littermates. The numbers of both NKP ($CD11b^-CD3^-NK1.1^-CD122^+$) and iNK ($CD11b^-CD3^-NK1.1^+CD122^+$) cells were substantially reduced in the male mice (Fig. 4C, 4D), suggesting that NK cell development was impaired in the males.

Abnormal expression of Sca-1 on hematopoietic cells in the bone marrow

We further examined the lymphoid, myeloid, and erythroid progenitor populations in the bone marrow of the mutant male mice. As shown in Fig. 5, it appeared that progenitor cells (defined as $lineage^-$ c-Kit^{hi} and Sca-1^-) of all of the indicated lineages in the mutant males were markedly reduced. However, Fig. 1B and 1F showed normal number of mature myeloid and erythroid cells in the mutant male mice. Interestingly, most $lineage^-$ cells in the mutant males strongly expressed the Sca-1 marker (*top panels* of Fig. 5A), which is commonly used to define the hematopoietic

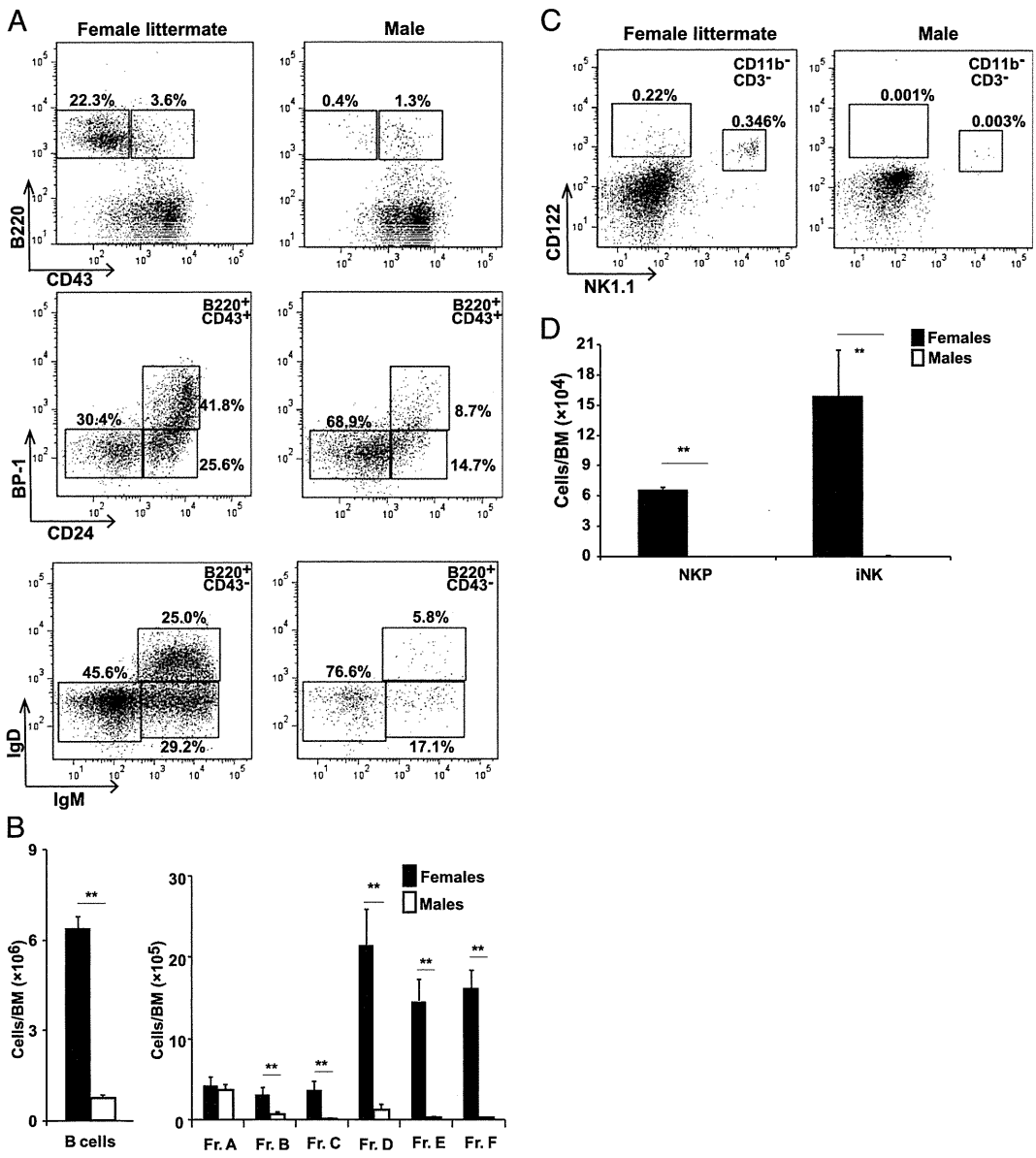

FIGURE 4. B and NK cell developments are arrested. Frequency (**A**) and number (**B**) of B cell subsets in the bone marrow at 6 wk of age. Hardy fractions in the bone marrow were gated as follows: $B220^+CD43^+BP\text{-}1^-CD24^-$ (A); $B220^+CD43^+BP\text{-}1^-CD24^+$ (A); $B220^+CD43^+BP\text{-}1^+CD24^+$ (A); $B220^+CD43^-IgM^-IgD^-$ (A); $B220^+CD43^-IgM^+IgD^-$ (A; and $B220^+CD43^-IgM^+IgD^+$ (B); the C' fraction ($B220^+CD43^+BP\text{-}1^+CD24^{hi}$) was not resolved. Data are representative from three independent experiments of five mice per genotype. Frequency (**C**) and number (**D**) of NKp ($CD122^+CD3^-CD11b^-NK1.1^-$) and iNK cells ($CD122^+NK1.1^+CD3^-CD11b^-$) are shown. Data are representative of four or five mice per genotype. $^{**}p < 0.01$.

progenitor or stem cells. Therefore, due to abnormally high expression of Sca-1, we may have been unable to exactly evaluate the hematopoietic progenitor cells in the mutant male mice.

The failure of adult B and NK lymphopoiesis is cell intrinsic

B cells and NK cells can be produced from bone marrow cells cultured in vitro on stromal cells, such as OP9 cells, in the presence of IL-7 or IL-15 (18, 19). To determine the cellular origin of the phenotype of the male mutant mice, we isolated HPCs, identified as Lin$^-$ (B220$^-$, Thy1$^-$, DX5$^-$, Ter119$^-$, Gr-1$^-$, CD11b$^-$) bone marrow cells, from the male mice and their female littermates. The HPCs were cultured on OP9 cells, with subsequently added cytokines. HPCs derived from the bone marrow of males did not produce NK (NK1.1$^+$) cells or B (CD19$^+$) cells, whereas significant NK and B cell populations were generated from the HPCs from female littermates (Fig. 6A).

To confirm this cell-intrinsic abnormality in vivo, we conducted bone marrow chimera experiments by transfusing a mixture of equal parts of wild-type (Ly5.1$^+$) and mutant (Ly5.2$^+$) bone marrow cells into lymphocyte-deficient *Il2rg*$^{-/-}$ mice. Consistent with the in vitro results, Ly5.2$^+$ bone marrow cells of mutant males failed to produce B or NK cells, whereas Ly5.1$^+$ wild-type HPCs fully reconstituted both B and NK cells in the same recipient mice (Fig. 6B). Transplanting wild-type bone marrow cells into irradiated mutant male mice rescued the B and NK cell deficiency (Fig. 6C), and PPs were also recovered 10 wk after the transplant (data not shown). This suggests that the PP deficiency is a result of the B cell deficiency and not an anlage defect. These results clearly indicate that the defect of B and NK cells in the mutant mice was intrinsic to hematopoietic cells.

Interestingly, the in vitro lymphopoiesis of B and NK cells from fetal liver HPCs was the same whether the HPCs were from the mutant males or their female littermates (Fig. 7A). Furthermore, the male fetal liver cells reconstituted B and NK cells in vivo, although at a lower level than cells from female littermates (Fig. 7B). Because fetal liver progenitors from the mutant males could produce B and NK cells, we compared the fetal B cell subsets and NK lymphopoiesis in male and female littermates at E17.5, when IgM$^+$ B cells and iNK are already present in wild-type mice (20, 21). As expected, we did not find a significant difference in the frequency of B or NK cells in the fetal liver of male and female littermate embryos (Fig. 7C). However, both B and NK cells derived from the male fetal liver disappeared by 10 wk after transplantation (data not shown). Nevertheless, the above results provide further evidence that the fetal B and NK cell development in the males was intact and that the NK and B cells detected in 3-wk-old males were generated from fetal liver progenitors.

In addition, male fetal liver cells could produce these lymphocytes even in male recipients (data not shown), supporting the conclusion that androgen does not contribute to the defect of B and NK cells in these mutant male mice.

EBF restores the precursor cells' ability to generate B220$^+$ B cells in mutant males

To address the molecular mechanisms for arresting the B cell development, we isolated prepro-B cells (Hardy fraction A) from the

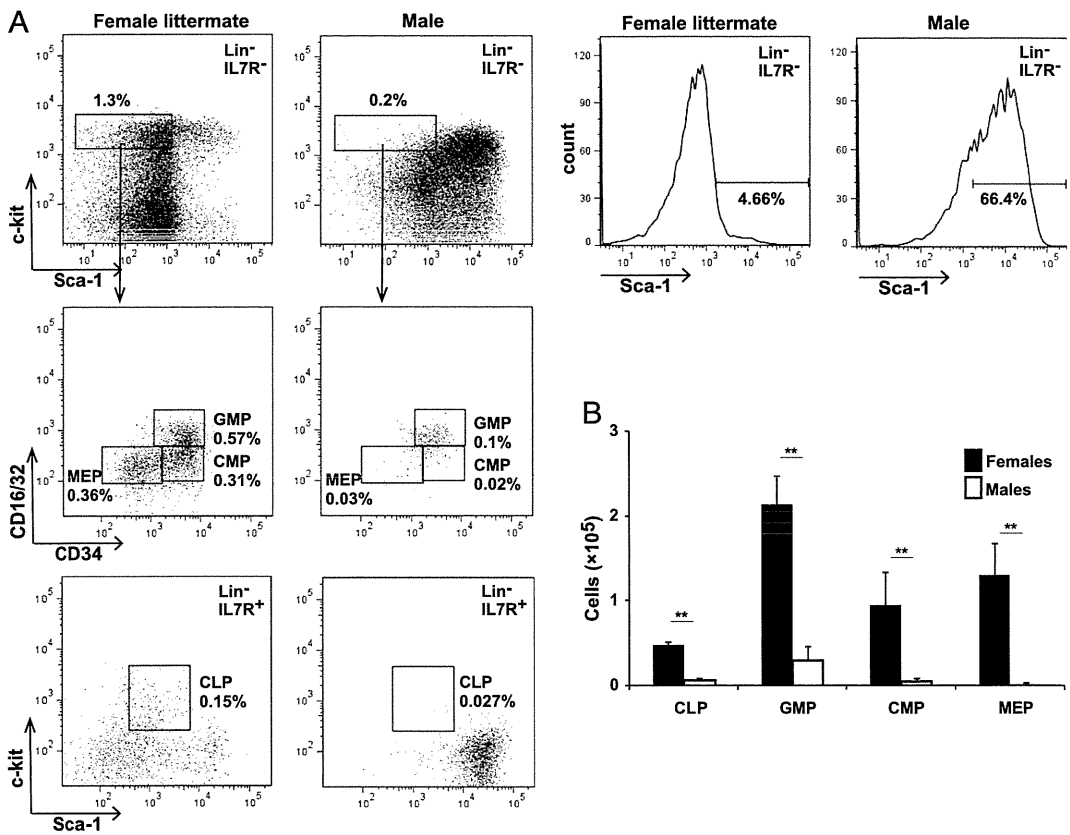

FIGURE 5. Abnormally high expression of Sca-1 on hematopoietic cells in the bone marrow. (**A**) Representative FACS analysis with the bone marrow cells from 12-wk-old mice are shown. Numbers in the FACS plots indicate the percentages of the indicated populations among total bone marrow cells. Each progenitor population was defined as bellow. The histogram shows expression of Sca-1 related to Lin$^-$CD127$^-$ gated cells. (**B**) The average absolute numbers of the indicated populations in the bone marrow are shown ($n = 3$ each). CLP: Lin$^-$CD127$^+$Sca1^{lo}c-Kit^{lo}; CMP: Lin$^-$CD127$^-$c-Kit^{hi}Sca1$^-$CD34$^{+/lo}$CD16/32^{int}; GMP: Lin$^-$CD127$^-$c-Kit^{hi}Sca1$^-$CD34$^+$CD16/32$^+$; and MEP: Lin$^-$CD127$^-$c-Kit^{hi}Sca1$^-$CD34$^-$CD16/32$^-$. $^{**}p < 0.01$.

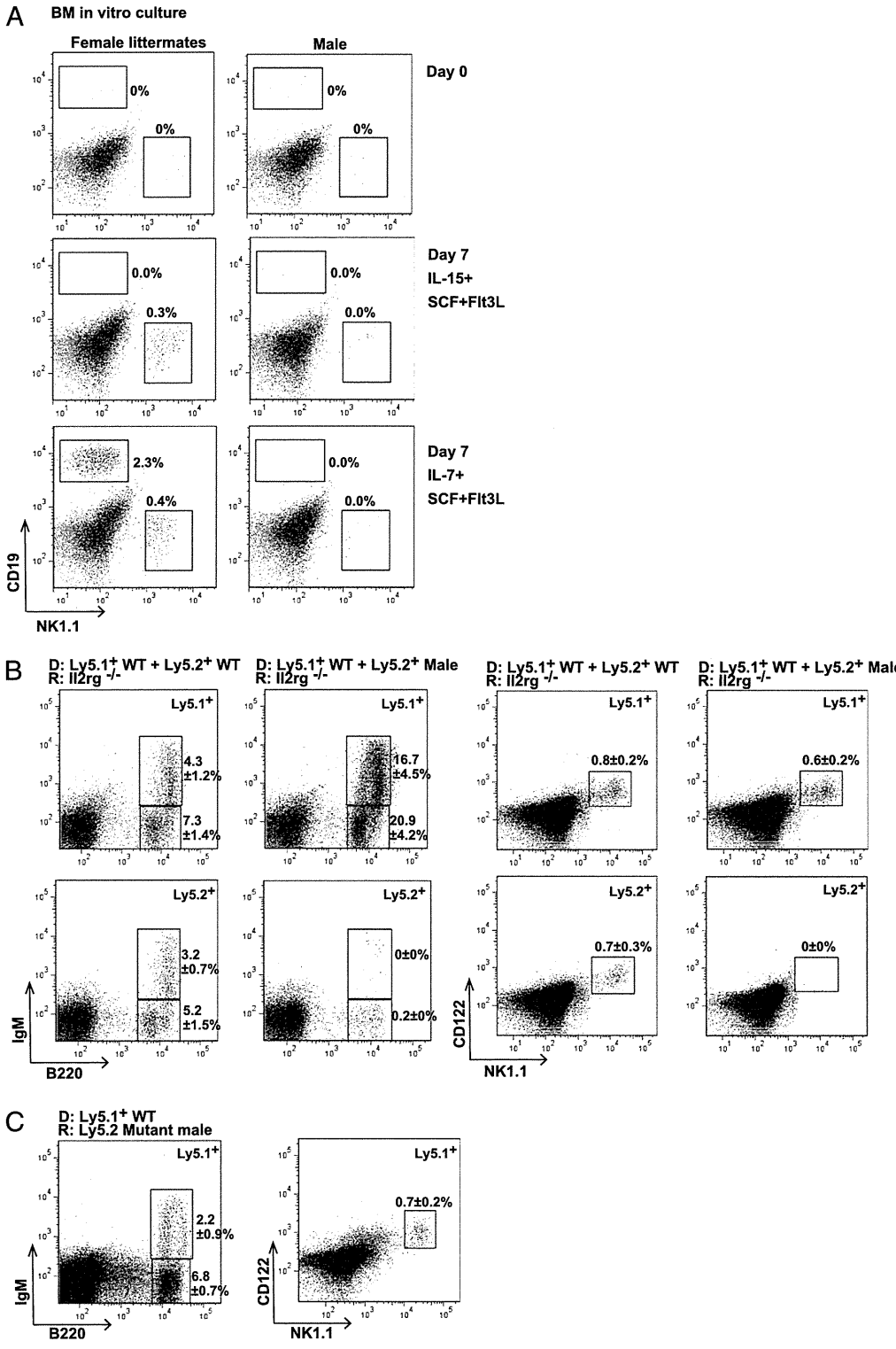

FIGURE 6. Cell-intrinsic failure of adult B cell and NK cell development. (**A**) In vitro differentiation of NK ($NK1.1^+$) and B ($CD19^+$) cells from bone marrow cells. HPCs ($B220^-$, $Thy1^-$, $DX5^-$, $Ter119^-$, $Gr\text{-}1^-$, $CD11b^-$) from the bone marrow of adult male or female littermates were cultured on OP9 stromal cells in the presence of exogenous cytokines. Numbers in plots indicate the percentages of live cells. Data are representative from two independent experiments. (**B**) B (*left panel*) and NK (*right panel*) cells generated in the bone marrow 8 wk after the reconstitution of irradiated $Il2rg^{-/-}$ recipients transfused with a 1:1 mixture of wild-type (Ly5.1) and wild-type (Ly5.2) or mutant male (Ly5.2) bone marrow cells. Numbers on each gate indicate the percentage relative to $Ly5.1^+$ or $Ly5.2^+$ cells. (**C**) Bone marrow cells from wild-type (Ly5.1) mice were transplanted into irradiated B cell–deficient mutant male mice (Ly5.2). B and NK cells in the bone marrow were analyzed 8 wk after reconstitution. Numbers on gates indicate the percentage relative to $Ly5.1^+$ cells. Data are from two independent experiments (n = 3 or 4 recipient mice per genotype). D, donor; R, recipient.

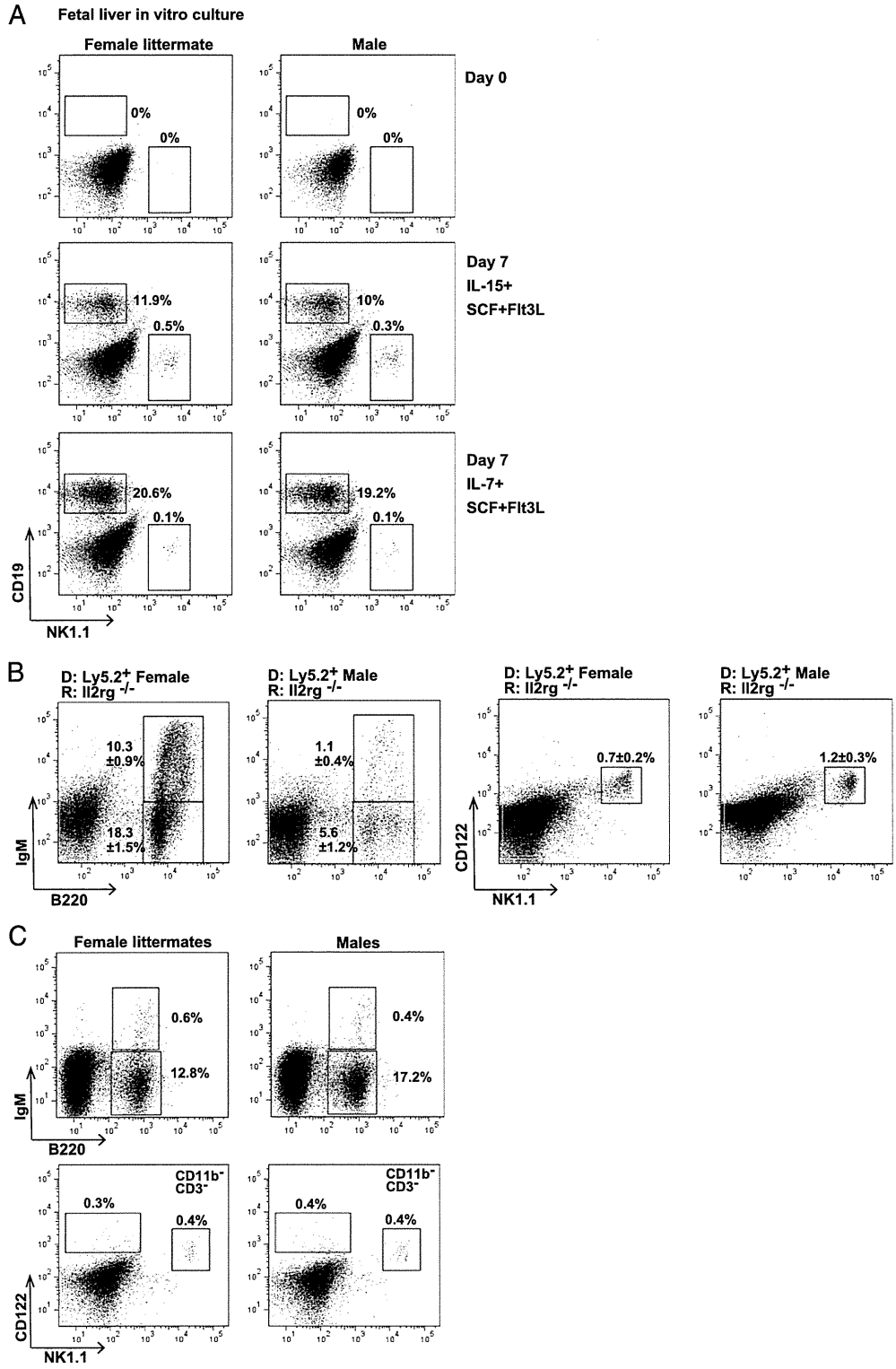

FIGURE 7. B and NK lymphopoiesis in the fetal liver is intact in the mutant males. (**A**) In vitro differentiation of NK ($NK1.1^+$) and B ($CD19^+$) cells from fetal liver cells. HPCs ($B220^-$, $Thy1^-$, $DX5^-$, $Ter119^-$, $Gr\text{-}1^-$, $CD11b^-$) from the fetal liver of male and female littermates were cultured on OP9 stromal cells in the presence of exogenous cytokines. Numbers in plots indicate the percentages of live cells. Data are representative from two independent experiments. (**B**) Female or male (Ly5.2) E17.5 fetal liver cells were injected into irradiated *Il2rg*$^{-/-}$ recipients. B (*left panel*) and NK (*right panel*) cell populations in the bone marrow were analyzed by FACS 4 wk after transplantation. (**C**) The percentage of B or NK cells in the E17.5 fetal liver of siblings produced from a mating between a B cell–deficient male mouse and a wild-type female mouse. Fractions A-D ($B220^+$ IgM^-), Fraction E ($B220^+IgM^+$), NKP ($CD122^+CD3^-CD11b^-NK1.1^-$), and iNK cells ($CD122^+NK1.1^+CD3^-CD11b^-$) were analyzed. Data are from two independent experiments with three or four recipient mice per genotype or two independent experiments pooled with five male or four female fetuses.

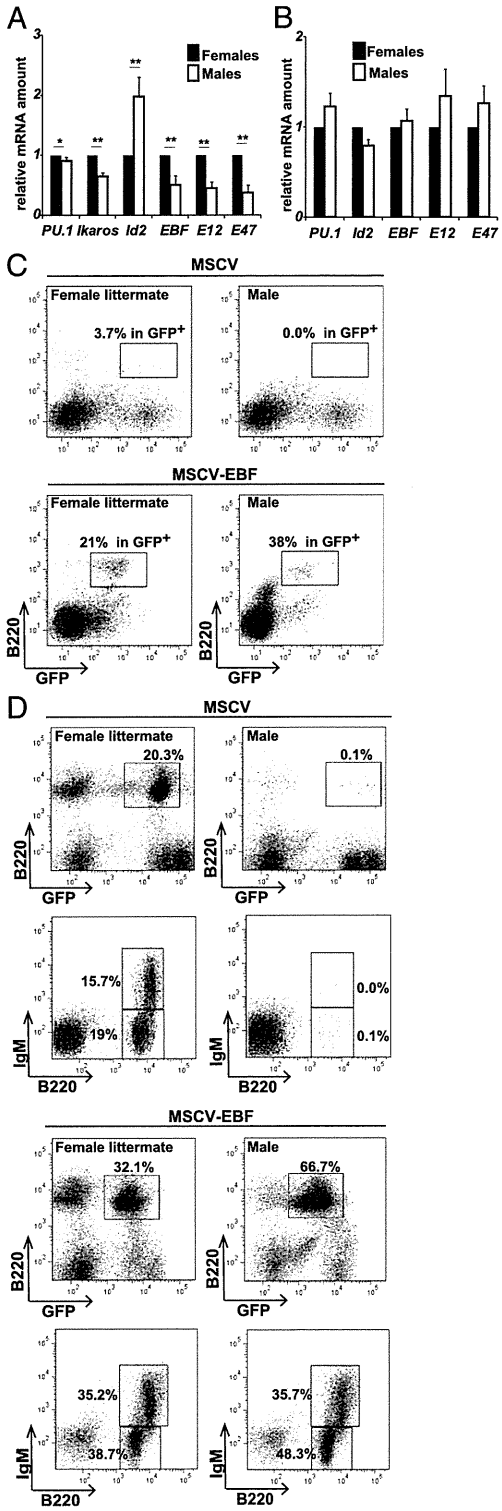

FIGURE 8. EBF restores B cell development in mutant male hematopoietic cells. The expression of genes involved in B cell development was analyzed in male and female littermates by real-time PCR. Hardy fraction A ($B220^+CD43^+BP\text{-}1^-CD24^-$) cells from adult bone marrow (**A**) or immature B ($B220^+IgM^-$) cells from the fetal liver (**B**) of male and female littermates were isolated by FACSAria II (BD Biosciences). Extracted RNA was reverse-transcribed and used for real-time PCR (see *Materials and Methods* for primers). All values were normalized to GAPDH and are presented as the fraction relative to cDNA from control mice (set as 1). Data show three independent experiments, each done in triplicate with pooled bone marrow from six mice or fetal liver from at least three mice per genotype. (**C**) Bone marrow HPCs were retrovirally transfected with a murine stem cell virus (MSCV; control) or MSCV-EBF and cultured on OP9 cells in the presence of SCF, Flt3L, and IL-7. Cells were analyzed by FACS 7 d postinfection to determine the B220 and GFP expression. Numbers in plots indicate the percentage relative to GFP^+ cells. A representative result from two independent experiments is shown. (**D**) Littermate female or male HPCs (Ly5.2) were infected with an MSCV or EBF retrovirus and injected into sublethally irradiated wild-type mice (Ly5.1). Bone marrow cells were analyzed for B220, IgM, and GFP expression by FACS. Numbers in plots indicate the percentage relative to Ly5.2 cells (*top panel*) or GFP^+ cells (*bottom panel*). A representative result from two independent experiments with three mice per group is shown. $*p < 0.05$, $**p < 0.01$.

adult bone marrow (Fig. 8A) or immature B cells ($B220^+IgM^-$) from the fetal liver (Fig. 8B) of male and female littermates. We used real-time RT-PCR to compare mRNA levels of essential transcription factors for B cell development. The transcription factors EBF and E2A (E12 and E47), both of which are essential for B cell development, were significantly decreased in the adult bone marrow (Fig. 8A) but not the fetal liver (Fig. 8B) of males as compared with females. However, there was a 2-fold increase in Id2, which is a transcriptional repressor for EBF and E2A, in the male adult bone marrow, although the fetal liver Id2 levels were comparable in males and females (Fig. 8A, 8B).

Because a lack of EBF or E2A causes B cell defects (22–24), the *EBF* or *E2A* gene was retrovirally transduced into mutant HPCs, which were then cultured on OP9-stroma cells under B cell differentiation conditions. Although the *E2A*-transduced male HPCs did not develop into $B220^+$ cells (data not shown), forced EBF expression successfully rescued the B cell development (Fig. 8C). *EBF* or a control vector was then retrovirally transduced into HPCs from male or female littermates ($Ly5.2^+$), and the HPCs were transplanted into irradiated wild-type mice ($Ly5.1^+$) for in vivo reconstitution. $B220^+$ B cells were not detected in recipient mice transfused with control vector–transfected HPCs from males, but were clearly reconstituted in recipients transfused with *EBF*-transduced (GFP^+) HPCs (Fig. 8D). Control recipients transfused with female HPCs transfected with either *EBF* or control genes showed clear $B220^+IgM^+$ B cell reconstitution (Fig. 8D). As EBF restricts lymphopoiesis in the B cell lineage by blocking the development of other lymphoid-derived cell pathways (25), *EBF* transfection did not result in the recovery of NK cells (data not shown). Collectively, forced EBF expression was able to rescue impaired B cell development, but not NK cell development, in the male mutant mice.

Discussion

In this study, we describe a novel mouse strain characterized by a male-specific defect of B cells, NK cells, and PPs. T cells, monocytes, granulocytes, and erythrocytes were relatively intact in these male mice. Most notably, this defect was linked to the Y chromosome. Mating the B cell–deficient males to wild-type females for several generations revealed that the B and NK cell deficiencies were inherited as Y chromosomal Mendelian characteristics. A multicolor FISH analysis demonstrated a structural abnormality in the Y chromosome.

We do not know how the Y chromosome abnormality mediates the B and NK cell defects. Because the female littermate mice, which do not have any genes encoded by Y chromosome, are immunologically normal, the immunodeficiency was not caused simply by the defect of a Y chromosome gene. Therefore, there are

at least three possible mechanisms: a gene that exists on another chromosome may be inserted into the Y chromosome and be overexpressed or ectopically expressed in B and NK cell precursors due to abnormally controlled gene expression. Another possibility is that a gene from another chromosome is translocated or inserted into the Y chromosome and forms a chimeric gene, which may produce an abnormal chimeric protein affecting B and NK cell differentiation. The third possibility is that a structural abnormality of the Y chromosome itself induces the ectopic expression of a Y chromosome gene in lymphocyte precursor cells, interfering with their differentiation.

To address the first possibility, we performed a multicolor FISH analysis and array-based comparative genomic hybridization to identify gene loci inserted from autosomes or the X chromosome into the Y chromosome. However, FISH analysis failed to show any abnormal signals on the Y chromosome (data not shown). Although we found copy-number abnormalities on three loci on chromosomes 2, 9, and 10, these did not appear to be associated with the Y chromosome (data not shown). To address the second possibility, we used a next-generation sequencer to sequence Y chromosome exons. However, we could not find any significant differences in the nucleotide sequence, including known single nucleotide polymorphisms, between the mutant males and control male mice kept in the same facility (data not shown). Therefore, chimeric gene formation is unlikely. Genomic sequencing of the entire Y chromosome would be necessary to completely rule out this possibility. However, unlike other chromosomal genes, the Y chromosome's many repetitive sequences make it difficult to analyze data from the next-generation sequencer. Thus, a new sequencing method is needed for the Y chromosome. To address the third possibility, we conducted microarray and real-time RT-PCR analyses of the Y chromosome gene expression in the bone marrow immature B cells of mutant and control male mice. These analyses also showed negative results (data not shown). Thus, the genetic mechanism for this novel Y chromosome–linked disease remains unclear.

B cell development is regulated by a transcriptional network consisting of, but not limited to, the transcription factors PU.1, Ikaros, E2A, EBF, Pax5, and Id2. PU.1 and Ikaros are critical for early lymphoid-lineage specification, whereas E2A, EBF, and Pax5 are essential for the commitment of common lymphoid progenitors to become B cells. Quantitative RT-PCR with prepro-B cells from the male mutant mice showed lower Ikaros, E2A, and EBF expression and higher Id2 expression (Fig. 8). Because Id2 is a physiologically relevant, negative EBF regulator, high Id2 levels may block B cell development in males at the prepro-B stage by suppressing EBF or/and E2A. As expected, deliberately expressing EBF in mutant male HPCs rescued the B cell differentiation, clearly indicating that an insufficient expression of EBF, likely induced by Id2 overexpression, may cause the B cell deficiency seen in the male mice. However, because the T cell Id2 levels were comparable in male and female littermates (data not shown), an *Id2* mutation cannot explain the abnormal Id2 expression in the prepro-B cells in the male mice. Further work is needed to clarify whether and how these genes are associated with B lymphopoiesis.

B and NK development from fetal liver cells was intact, whereas that from bone marrow was severely impaired in the male mice. Few molecules have been reported to act in such a way, with IL-7 and IL-7R being the prototypical examples (26). Because Flt3 (also called FLK2) signal can compensate IL-7 signal in the fetal liver, B lymphopoiesis is independent of IL-7 in the fetal liver, which is indispensable for that in bone marrow (27, 28). However, no study has shown that fetal and adult NK cell development is regulated by distinct cytokine signal or transcription factors. The age-dependent defect of NK cells in mutant males sheds light on the new aspect of the NK cell development.

IL-7 requirement between B1- and B2-B cell lymphopoiesis is different. As described above, B2-B cell development from bone marrow is dependent on IL-7, whereas IL-7 is indispensable for B1-B cell development, which is rather promoted in IL-7 deficient mice (29). Therefore, although the age-dependent B2-B cell defect in the mutant mice resembles that in IL-7–deficient mice, the defect of both B1- and B2-B cells in the mutant mice cannot be explained by the IL-7/Flt3 compensation mechanism. Thereby, the immunodeficient phenotype of the mutant mice suggests a unknown pathway, which is shared by B1-B, B2-B, and NK lymphopoiesis.

Among immunodeficiencies, it is rare to see a combined B and NK immunodeficiency accompanied by normal T cells. Several common factors are essential for B and NK lymphopoiesis, such as Ikaros, PU.1, and cytokine signals. NK development depends on IL-15, because both *IL15*$^{-/-}$ and IL-15R α-chain–deficient mice (*IL-15Rα*$^{-/-}$) lack peripheral NK cells and NK cell–mediated cytotoxicity (30, 31) IL-7, which shares a γ-chain with IL-15, is essential for B cell development. However, NKP cells are generated from HSCs independently of IL-15 or any γc cytokines (32). Therefore, an abnormality in γ-chain cytokines and their intracellular signals might not cause the immunodeficient phenotype in our mice. Interestingly, a previous study reported that mice with a C-terminal Ikaros deletion (Ikaros C-null knockout mice), like our mice, have T cells but are deficient in B and NK cells (33). A combined immunodeficiency syndrome in humans, characterized by adult-onset B and NK cell deficiencies with normal T cells, was recently reported in a female patient (34). However, the T cell responses were aberrantly hyper in both the patient and in Ikaros-mutant mice, whereas the in vitro T cell responses in our male mutant mice appeared relatively normal (data not shown). Therefore, the combined immunodeficiency of B and NK cells in our mice is a novel phenotype, suggesting an unknown molecular mechanism shared by B and NK cell development.

The mutant male mice showed a marked reduction of lineage$^-$c-Kit^{hi}Sca-1$^-$ cell populations in the bone marrow. However, because the absolute number of the late progenitors and mature populations of myeloid and erythroid lineages were normal in the mutant male mice, the mutant mice should have the functional hematopoietic progenitor cells. Similarly, functional common lymphoid progenitor cells may also exist in the male mice because they have a normal number of prepro-B cells. These results suggest that the early progenitors in the bone marrow of the mutant mice cannot be defined by the conventional commonly used marker Sca-1. The possible effect of Sca-1 overexpression on B and NK cell differentiation will be required.

This is the first report, to our knowledge, of a Y-linked immunodeficiency. Identifying the target substrate or affected pathway would help us determine the Y chromosome's exact contribution in lymphocyte development. Males from our novel strain will provide a key experimental model for studying possible common factors that are responsible for B and NK lymphopoiesis but do not contribute to T cell development in adults.

Acknowledgments

We thank the Biomedical Research Core and the Institute for Animal Experimentation (Tohoku University Graduate School of Medicine) for technical support. We also thank Dr. K. Kikuchi (Victor Chang Cardiac Research Institute, New South Wales, Australia) for technical advice.

Disclosures

The authors have no financial conflicts of interest.